m⁶A demethylase ALKBH5 promotes tumor cell proliferation by destabilizing IGF2BPs target genes and worsens the prognosis of patients with non-small cell lung cancer

Kazuo Tsuchiya[1,2], Katsuhiro Yoshimura[1,2], Yuji Iwashita[1], Yusuke Inoue[1,2], Tsutomu Ohta[1,3], Hirofumi Watanabe[1,2], Hidetaka Yamada[1], Akikazu Kawase[4], Masayuki Tanahashi[5], Hiroshi Ogawa[6], Kazuhito Funai[4], Kazuya Shinmura[1], Takafumi Suda[2], Haruhiko Sugimura[1*].

Corresponding author:

Haruhiko Sugimura, MD, Ph.D., Department of Tumor Pathology, Hamamatsu University School of Medicine, 1-20-1 Handayama Higashi-ku, Hamamatsu, Shizuoka 431-3192 Japan. Tel: +81-53-435-2220; Fax: +81-53-435-2225; E-mail: hsugimur@hama-med.ac.jp

Abstract

1

Background: The modification of N^6-methyladenosine (m^{6}A) in RNA and its eraser ALKBH5, an m^{6}A demethylase, play important roles across various steps of human carcinogenesis. However, the involvement of ALKBH5 in non-small cell lung cancer (NSCLC) development remains to be completely elucidated.

Methods: The current study investigated the involvement of ALKBH5 in NSCLC development using immunostaining of clinical NSCLC specimens as well as cancer-related cellular functions (cell proliferation, migration ability, cell cycle, and apoptosis) in ALKBH5-knockdown lung cancer cell lines. Moreover, a microarray was utilized to comprehensively analyze mRNA and m^{6}A in ALKBH5-knockdown cells. m^{6}A target genes were identified using the methylated RNA immunoprecipitation (MeRIP) assay with m^{6}A antibody. Furthermore, mRNA stability and protein expression owing to m^{6}A modification (the target genes) were examined.

Results: Clinicopathological analysis revealed that increased ALKBH5 expression was an independent prognostic factor associated with unfavorable overall survival in NSCLC (hazard ratios, 1.468; 95% confidence interval, 1.039–2.073). *In vitro* study revealed that ALKBH5 knockdown suppressed cell proliferation ability of PC9 and A549 cells as well as promoted G1 arrest and increased the number of apoptotic cells. Furthermore, ALKBH5 overexpression increased the cell proliferation ability of the

immortalized cell lines BEAS2B and HEK293. Comprehensive analysis of microarray and MeRIP quantitative-polymerase chain reaction revealed that 3′ untranslated regions (3′ UTRs) of CDKN1A, TIMP3, E2F1, and CCNG2 mRNA were potential targets of ALKBH5. Depending on the lung cancer cell lines, increased expression of CDKN1A or TIMP3 and decreased cell proliferation were observed by ALKBH5 knockdown. These alterations were offset by a double knockdown of both ALKBH5 and one of the IGF2BPs. The decline of mRNAs was, at least partly, owing to the destabilization of these mRNAs by one of the IGF2BPs.

Conclusions: Upregulation of ALKBH5 in NSCLC reduces m^{6}A modifications on the 3′ UTR of specific genes. Loss of m^{6}A causes a decrease in opportunity for recognition by IGF2BPs and destabilizes the target transcript, such as CDKN1A (p21) and TIMP3. Downregulation of CDKN1A (p21) and TIMP3 induces cell cycle alteration and inhibits apoptosis. The ALKBH5–IGF2BPs axis promotes cell proliferation and tumorigenicity, which in turn causes the unfavorable prognosis of NSCLC.

Keywords: Non-small cell lung cancer (NSCLC), m^{6}A, ALKBH5, IGF2BPs, CDKN1A (p21), TIMP3

Background

Lung cancer, the incidence of which has continued to increase annually,

remains the most frequently diagnosed cancer and leading cause of cancer-related death

worldwide [1]. Considering the rapid improvement in the treatment of lung cancer,

particularly non-small cell lung cancer (NSCLC), physicians now have several options

of personalized treatments targeting driver genes, such as EGFR mutations, ALK

rearrangements, ROS1 rearrangements, and BRAF mutations or combination therapies

comprising immunotherapy and anticancer drugs [2-6]. However, despite the current

advancements in precision medicine, NSCLC still exhibits poor long-term prognosis

and high mortality rates owing to the rapid growth, metastasis, and infiltration of cancer.

Therefore, identifying effective therapeutic targets that inhibit such malignant behaviors

of NSCLC is urgently needed.

N^6-methyladenosine (m^{6}A), the most prevalent internal messenger RNA (mRNA)

modification, controls various mRNA functions. The m^{6}A sites, which are widely

distributed around the stop codons and 3′ untranslated regions (UTRs) of mRNAs,

presumably exist in precursor mRNAs [7]. Recent m^{6}A transcriptome analysis revealed

that m^{6}A is predominantly present in the RRACU (R = A/G) consensus motif of

mammals [8]. m^{6}A is reversibly catalyzed by a methyltransferase complex (writer) and

4

demethylase (eraser). Accordingly, the methyltransferase complex comprises

methyltransferase-like 3 and 14 (METTL3 and METTL14) with their cofactors Wilms

tumor 1-associated protein (WTAP), VIRMA (KIAA1429), and RNA-binding motif

protein 15 (RBM15) [9-12]. Further, fat mass and obesity-related protein (FTO) and

AlkB homolog 5 (ALKBH5) have been identified as two eukaryotic demethylases that

oxidatively demethylate m^6A with α-ketoglutarate as a substrate and Fe (II) as a

coenzyme [13, 14]. FTO is also involved in the demethylation of

N^6,2'-O-dimethyladenosine (m^6A_m), whereas other than m6A, there is no other RNA

that is demethylated by ALKBH5 [15, 16]. Moreover, m^6A-binding protein (reader

protein), which recognizes m^6A, is involved in numerous biological processes in an

m^6A-dependent manner. For instance, YT521-B homology (YTH) domain containing 1

(YTHDC1) and YTHDC2 promote alternative splicing and mRNA export from the

nucleus to the cytoplasm [17-21]; heterogeneous nuclear ribonucleoprotein G

(HNRNPG) alters RNA structures via RNA–protein interaction [22, 23]; YTH domain

family1 (YTHDF1), YTHDF3, METTL3, and eukaryotic initiation factor3 (eIF3)

regulate translation efficiency [24-27]; and insulin-like growth factor 2 mRNA-binding

proteins (IGF2BPs), YTHDF2, YTHDF3, and YTHDC2 alter mRNA stability [27-30].

5

Over the past few years, several researchers investigating the role of m^6A eraser in malignant tumors have revealed that m^6A eraser proteins play a critical role in oncogenesis. A number of previous studies have demonstrated that ALKBH5 exerts a cancer-promoting effect in glioblastoma, osteosarcoma, colon cancer, ovarian cancer, esophageal squamous cell carcinoma, endometrial cancer, and renal cell carcinoma [31-37]. In contrast, ALKBH5 has been reported to play a tumor-suppressing effect in hepatocellular carcinoma and pancreatic cancer [38, 39]. Several studies on lung cancer have shown that FTO plays a cancer-promoting role through m^6A modification in lung squamous cell carcinoma and adenocarcinoma [40-42], whereas ALKBH5 inhibits NSCLC tumorigenesis by reducing YTHDFs-mediated YAP expression [43]. Conversely, ALKBH5 had also been found to promote NSCLC progression by regulating TIMP3 stability [44]. Thus, the precise role of ALKBH5 in NSCLC tumorigenesis across various conditions deserves further investigation.

Cell type and cell environment (e.g., during hypoxic conditions) as well as the m^6A target gene and its recognition protein (reader) have been found to affect RNA metabolism caused by ALKBH5 perturbation [45, 46]. Therefore, m^6A-mediated gene expression regulated by ALKBH5 could result in various consequences in cancer cells depending on the surrounding environment and other factors. Several studies regarding

6

m^6A have focused on specific genes in the specific contexts, with their results showing

that m^6A is involved in the mechanisms through which these specific genes are

regulated. However, in actual human cancers, ALKBH5 catalyzes specific m^6A of

numerous genes, which simultaneously alters several RNA and protein expressions

through RNA recognition by reader proteins, consequently causing numerous

interactions between them *in vivo*. As such, systematically clarifying the association

between m^6A modification and cancer development across each clinical and

pathological setting is important. Furthermore, elucidating the significance of m^6A

modification by ALKBH5 may facilitate the clinical usage of such molecules as

therapeutic targets. Therefore, the current study aimed to examine the role of m^6A

demethylase in NSCLC focusing on ALKBH5 and determine its association with

downstream targets, including "readers" and "target genes."

Methods

Immunohistochemistry

Resected NSCLC samples from Hamamatsu University School of Medicine and Seirei

Mikatahara General Hospital were collected and named as the HUSM cohort. Tissue

microarray (TMA) sections were analyzed using immunohistochemistry (IHC) as

previously described [47]. Cores of insufficient quality or quantity were excluded from analysis. Antibodies for ALKBH5 (HPA007196, Atlas Antibodies, Stockholm, Sweden) and FTO (Ab124892, Abcam, Cambridge, UK) were diluted at 1:400, whereas those specific for EGFR E746-A750 deletion (#2085, D6B6, Cell Signaling Technology [CST], Danvers, MA, USA) and EGFR L858R mutant (#3197, 43B2, CST) were diluted at 1:100, followed by incubation at room temperature for 0.5 h. Protein expression levels were then assessed using the H-score, which was calculated by multiplying the percentage of stained tumor area (0%–100%) by the staining intensity (scored on a scale of 0–3) to yield a value ranging from 0 to 300 as previously described [48].

Analysis of publicly available datasets

We used the lung cancer database in the Kaplan–Meier plotter (http://kmplot.com/analysis/index.php? p=service&cancer=lung) to analyze the association between prognosis and ALKBH5 and FTO mRNA expression in NSCLC cohorts. Data were downloaded on December 10, 2020. Kaplan–Meier curves for overall survival (OS) were generated and stratified according to the median expression of each mRNA. To assess the mRNA expression of ALKBH5 and FTO, data from the

Cancer Genome Atlas (TCGA) (NSCLC, Provisional) were downloaded from

cBioPortal (http://www.cbioportal.org/) on November 11, 2019. Expression data were

obtained in the form of RNA-seq by Expectation Maximization (RSEM).

Immunofluorescence analysis

Cells grown on coverslips were fixed with 4% paraformaldehyde and permeabilized

with 0.1% Triton X-100. After blocking with 5% bovine serum albumin in PBS (−) at

room temperature for 1 h, the cells were probed with primary antibodies against

ALKBH5 (HPA007196, Atlas Antibodies) and then incubated with a Goat anti-Rabbit

IgG (H + L) Cross-Adsorbed Secondary Antibody, Alexa Fluor 546 (#A-11010,

Thermo Fisher Scientific, Waltham, MA, USA). Nuclei were stained with ProLong®

Gold Antifade Reagent with DAPI (#8961, CST), after which the cells were imaged via

fluorescence microscopy using z-stack image reconstructions (BZ-9000; Keyence,

Osaka, Japan).

Cell lines and transient knockdown with siRNA

The human lung cancer cell lines H1299, H460, H2087, A549, ABC1, and H358 and

the human immortalized cell lines BEAS2B and HEK293 were obtained from Health

Science Research Resources Bank (Osaka, Japan) or the American Type Culture

Collection (Manassas, VA, USA). PC3 and PC9 lung cancer cells were purchased from

the Japanese Collection of Research Bioresources Cell Bank (Osaka, Japan) and

RIKEN BioResource Center (Tsukuba, Japan), respectively, whereas ACC-LC176 cells

were a kind gift from Dr. Takashi Takahashi (Nagoya University) [49]. RERF-LC–MS,

HLC-1, and LC-2/ad were kind gifts from Dr. Toshiro Niki (Tokyo University) [50].

Lung cancer cell lines were cultured in RPMI1640 medium (R8758, Thermo Fisher

Scientific), whereas HEK293 cells were cultured in DMEM (D5796 MERCK,

Darmstadt, Germany) containing 10% (vol./vol.) fetal bovine serum (FBS), 100 IU/mL

penicillin G, and 100 µg/mL streptomycin. LHC9 (12680013, Thermo Fisher

Scientific) was also used as a medium for BEAS2B cells. Cells were maintained in a

5% CO_2 and 95% air incubator at 37□. Silencer Select Pre-designed siRNA for

ALKBH5 (siALKBH5: s29743, s29744, s29745, Invitrogen), FTO (siFTO: s28147,

s28148, s28149, Invitrogen), IGF2BP1(siIGF2BP1: s20916, s20917, Invitrogen,

Carlsbad, CA, USA), IGF2BP2 (siIGF2BP2: s20922, s20923, Invitrogen),

IGF2BP3(siIGF2BP3: s20919, s20920, Invitrogen), and Silencer Select Negative

control (siNC: 4390843, Invitrogen) were purchased for transient knockdown. More

than two different sequences were used for one target gene to minimize off-target

10

effects. Cells were cultured for 24 h before transfection, after which they were

transfected with 15 nM of final siRNA concentrations using Opti-MEM (31985070,

Gibco, Dublin, Ireland) and Lipofectamine® 2000 (11668019, ThermoFisher). The cells

were then used for further assays at 48–96 h after transfection. When no siRNA sample

number was available, siRNA no. 1 (#1) and siRNA no. 3 (#3) were pooled for

ALKBH5 unless otherwise specified. siIGF2BP1, siIGF2BP2, and siIGF2BP3 were

pooled for all transfections.

Generation of Retro-X Tet-On inducible cell lines overexpressing ALKBH5

The retroviral plasmid pRetroX-TetOne puro (634307, Clontech, Mountain View, CA,

USA) was amplified using NEB Stable competent *Escherichia coli* (high efficiency)

(C3040H, NEW ENGLAND BioLabs, Ipswich, MA, USA). The full-length ALKBH5

sequence (NM_017758), which was confirmed using Sanger sequencing, was subcloned

into pRetroX-TetOne puro vector using EcoRI and BglII restriction sites

(pRetroX-TetOne puro-ALKBH5). Retroviral supernatants were produced using the

GP2-293 packaging cell line (Clontech), in which pRetroX-TetOne puro empty vector

or pRetroX-TetOne puro-ALKBH5 were each cotransfected with the envelope vector

VSV-G using Xfect transfection reagent (Clontech). BEAS2B, HEK293, PC9, and

A549 cells were transfected for 24 h using 4 µg/mL polybrene (H9268, Sigma-Aldrich,

St. Louis, MO, USA). Puromycin selection (0.5–1.5 µg/mL) began 48 h after

transfection and lasted for 3 days until all non-transfected cells had died. In subsequent

experiments, Retro-X cells were induced with 0.1–100 ng/mL of doxycycline (DOX)

diluted in culture media upon cell seeding for 24–96 h. Cells transfected with

pRetroX-TetOne puro-ALKBH5 with 100 ng/mL DOX were designated as

ALKBH5-overexpressed (OE) cells, whereas those infected without DOX were

designated as negative control (NC) unless otherwise noted.

RNA isolation and quantitative-polymerase chain reaction (qPCR)

Total RNA was extracted using the RNeasy Plus Mini Kit (#74136, QIAGEN, Hilden,

Germany) according to the manufacturer's instructions, with the total RNA

concentration calculated using Nanodrop (NanoDrop1000, Thermo Fisher Scientific).

cDNA was synthesized from 1 µg of total RNA using the ReverTra Ace qPCR RT

Master Mix (FSQ-201, TOYOBO) according to the manufacturer's instructions. qPCR

reactions were performed on a Step One Plus Real-Time PCR System (Applied

Biosystems, Thermo Fisher Scientific) using the THUNDERBIRD qPCR Mix

(QPS-201, TOYOBO, Osaka, Japan). The relative RNA expression levels were

calculated using the ΔΔCt method, with the levels normalized to glyceraldehyde

3-phosphate dehydrogenase (GAPDH) mRNA. All amplicons were confirmed as a

single product using agarose gel visualization and/or melting curve analysis. The

applied primer sequences are listed in Table S1.

Protein isolation and western blotting

Total protein lysates were extracted from whole cells using $1\times$ sodium dodecyl sulfate

(SDS) sample buffer. The Pierce BCA Protein Assay Kit (Cat#23225, Thermo Fisher

Scientific) was used to determine the protein concentration. All proteins were separated

using SDS-polyacrylamide gel electrophoresis and transferred to PVDF Blotting

Membrane (P 0.45, A29532146, GE healthcare Life science, Chicago, IL, USA) using

the Trans-Blot Turbo Cassette (Bio-Rad, Hercules, CA, USA). Blocking One (03953,

Nacalai, Kyoto, Japan) or 5% skimmed milk were used for blocking. Primary antibodies

for ALKBH5 (1:1000 dilution, HPA007196; Atlas Antibodies), FTO (1:1000 dilution,

Ab124892; Abcam), IGF2BP1 (1:1000 dilution, 22803-1-AP; Proteintech), IGF2BP2

(1:1000 dilution, 11601-1-AP; Proteintech), IGF2BP3 (1:2000 dilution, 14642-1-AP;

Proteintech), TIMP3 (1:3000 dilution, Ab39184; Abcam), p21 (1:1000 dilution, A1483;

ABclonal, Woburn, MA, USA), E2F1 (1:500 dilution, A2067; ABclonal), CCNG2

(0.2μg/mL, Ab251826; Abcam), p53 (1:200 dilution, Sc-126; SANTA CRUZ BIO

TECHNOLOGY, Dallas, TX, USA), and GAPDH (1:1000 dilution, Ab8245; Abcam)

were incubated for overnight at 4□. Secondary antibodies for rabbit (1:20000 dilution,

NA9340; GE healthcare Life science) or mouse (1:20000 dilution, NA9310; GE

Healthcare Life Science) were incubated at room temperature with 1%–5% skimmed

milk for 1 h. Enhanced chemiluminescence (Pierce ECL Plus Substrate or West Atto

Ultimate Sensitivity Substrate, Thermo Fisher Scientific) was used to visualize the

protein bands using ChemiDocTouch (Bio-Rad).

Cell viability assay

Cells were seeded into 96-well plates with 3000 cells per well after 48 h of knockdown

or overexpression. Cell proliferation was monitored using Cell Counting Kit-8 (CCK-8;

Dojindo, Kumamoto, Japan) according to the manufacturer's protocol. Thereafter, the

cells were incubated with 10% CCK-8 for 1 h, followed by absorbance assessment at

450 nm in each well via spectrophotometry (Synergy HT, BioTek, Winooski,VT, USA)

every 24 h.

Transwell migration assay

Cell migration was evaluated using a 24-well plate with cell culture inserts (353097, Falcon, Mexico City, Mexico) containing a filter with 8 μm-diameter pores. Briefly, after serum starvation for 24 h with 0.1% FBS-containing RPMI1640 medium, 1×10^5 cells resuspended in 500 μL of RPMI1640 medium (Gibco) were seeded into the upper chamber, after which RPMI1640 medium containing 10% FBS was placed in the lower compartment of the chamber. After incubation for 16 h, the upper surface of the membrane was wiped with a cotton-tipped applicator to remove non-migrating cells, whereas the migrating cells on the lower surface were fixed with cold methanol and stained with 0.5% crystal violet. Migrating cells were automatically counted in three random microscopic fields using the Hybrid Cell Count software (BZ-□ Analyzer, Keyence, Osaka, Japan).

Wound-healing assays

To assess cell migration, 2×10^5 cells were seeded into 6-well plates. Thereafter, cells were incubated in 5% CO_2 at 37□ for 48□h and an additional 24 h with 0.1% FBS-containing RPMI1640 medium. A wound was scratched into the cells using a 200-μL plastic tip and washed with PBS (–). The cells were then incubated in RPMI1640 containing 10% FBS. The relative distance of the scratches was observed

under an optical microscope (IX53, Olympus, Tokyo, Japan) at 3–6 time points after wounding and assessed using the Image J software [51].

Cell cycle assay and apoptosis assay

Cell Cycle Assay Solution Blue (C549, Dojindo) was used to measure the cell cycle according to the manufacturer's instructions. Briefly, treated cells were synchronized at the G1 phase through serum starvation with 0.1% FBS-containing medium for 48 h. At 24 h after the release of serum starvation, the treated cells were collected, washed with PBS (−), and incubated with 5 μL cell cycle assay solution for 15 min at 37□. Thereafter, DNA content was determined based on staining intensity using a Gallios flow cytometer (Beckman Coulter, Miami, FL, USA). The Annexin V-FITC Apoptosis Detection Kit (15342-54 Nacalai) was used to detect apoptosis by measuring annexin V and propidium iodide (PI)-positive cells following the manufacturer's instructions. Briefly, cells were incubated for 96 h after siRNA transfection. To induce apoptosis, the cells were exposed to either 7.5 μM of gefitinib (078-06561, FUJIFILM) or 10 μM of cisplatin (P4394, Sigma-Aldrich) alone for 48 h after siRNA transfection. The treated cells were collected, washed with PBS (−), and incubated with 5 μL of annexin V-FITC solution and 5 μL of PI solution for 15 min. Thereafter, apoptotic cells were determined

16

using a Gallios flow cytometer. Results were analyzed using the FlowJo software

(Becton, Dickinson, Franklin Lakes, NJ, USA), after which the extent of apoptosis and

cell cycle distribution were determined.

RNA stability assay

Cancer cells were incubated for 48 h after siRNA transfection. Cells were treated with

actinomycin D at a final concentration of 5 µg/mL. Total RNA was extracted at 0, 2, 4,

and 6 h after adding actinomycin D. The remaining CDKN1A and TIMP3 mRNA was

measured through quantitative real-time PCR and normalized to RPL32 mRNA, which

has a half-life of 25 h [52].

Quantitative analysis of global m⁶A levels using liquid chromatography–mass

spectrometry/mass spectrometry (LC–MS/MS)

PolyA-enriched RNA was extracted using PolyATract mRNA isolation systems

(#Z5310 Promega, Madison, WI, USA) according to the manufacturer's instructions.

PolyA-enriched RNA concentration was calculated using Qubit 2.0. The

polyA-enriched RNA was enzymatically hydrolyzed using 8-OHdG Assay Preparation

Reagent Set (292-67801, FUJIFILM Wako Pure Chemical Corporation, Tokyo, Japan).

Technically, 100 ng of polyA-enriched RNA was digested using 5.7 μL of acetic acid buffer and 3 μL of Nuclease P1 included in the 45-μL sample containing nuclease-free water at 37□ for 30 min, followed by incubation with 6 μL of Tris Buffer and 0.3 μL of alkaline phosphatase at 37□ for 30 min. After digestion, the sample was centrifuged at 14,000 g and 4□ for 20 min using a Nanosep 3K Omega centrifugal device (Pall Corporation, Port Washington, NY, USA) according to a previously published method [53].

As an internal standard, N^6-methyladenosine-d3 (m^{6}A-d3; M275897, Toronto Research Chemicals, Toronto, Canada), which is a stable isotope of N^6-methyladenosine labeled with three deuterium atoms on the N^6-methyl group, was added to the nucleosides obtained via digestion of polyA-enriched RNA. These nucleosides were separated using an Acquity UPLC HSS T3 column (2.1 mm × 100 mm; Waters, Milford, CT, USA) with 0.1% (vol./vol.) formic acid in water as mobile phase A and methanol as mobile phase B at a flow rate of 200 μL/min in a linear gradient elution of 5%–60% B from 0 to 7 min. Standard compounds of adenosine (A; A9251, Sigma-Aldrich), N^6-methyladenosine (m^{6}A; A170736, Sigma-Aldrich), and m^{6}A-d3 were used to confirm the nucleoside-to-base ion mass transitions of 268.1–136.4 (A), 282.2–150.2 (m^{6}A), and 285.2–153.2 (m^{6}A-d3). Peak areas of A, m^{6}A, and m^{6}A-d3 in the

18

nucleosides digested from polyA-enriched RNA were calculated using the column

retention time of the standard compounds using Analyst 1.6.1 software (AB SCIEX,

Foster City, CA, USA). The m^6A level was quantified as the ratio of m^6A to A or

m^6A-d3 based on the calibrated concentrations.

Microarray analysis of differentially expressed genes

Total RNA was extracted from ALKBH5-knockdown or control PC9 cells 96 h after

transfection. RNA samples were used for global gene expression profiling on human

Clariom S Assay microarrays (Thermo Fisher Scientific, Wilmington, DE, USA), which

include 24351 genes. All microarray analyses were entrusted to Filgen Inc. (Aichi,

Japan). A total RNA quality control check was performed using a NanoDrop ND-1000

(Thermo Scientific) and an Agilent 2100 Bioanalyzer. Using the Gene Chip TM WT

PLUS Reagent Kit, fragmented and labeled cDNA samples were prepared from 250 ng

of total RNA according to the manufacturer's instructions (Gene Chip TM WT PLUS

Reagent Kit User Manual). Thereafter, 100 μL of hybridization solution was prepared

using 73 μL of Hybridization Master Mix and 2.3 μg of fragmented and labeled cDNA.

The array was incubated using the Gene Chip TM Hybridization Oven 645 at 45□ for

16 h (60 rpm). The array was cleaned using the Gene Chip TM Fluidics Station 450 and

19

scanned using the Gene Chip TM Scanner 3000 7G according to the manufacturer's

instructions [Gene Chip TM Command Console (AGCC) 4.0 User Manual]. The

Microarray Data Analysis Tool version 3.2 (Filgen, Aichi, Japan) was used for data

normalization and subsequent processing. Differentially expressed mRNAs were

identified using a set cutoff (fold change > 1.5 or < 0.67; $P < 0.01$). Gene set

enrichment analysis (GSEA) was performed to examine the gene set regulated by

ALKBH5 knockdown (http:/software.broadinstitute.org/gsea/omdex.jsp) [54]. For

analysis, the false discovery rate (FDR) based on gene set permutation was used.

Microarray data has been deposited in the Gene Expression Omnibus (GEO) at the

National Center for Biotechnology Information (NCBI) (accession number

GSE165453).

Epitranscriptomic microarray analysis

Unfragmented total RNA was extracted from ALKBH5-knockdown or control PC9

cells at 96 h after transfection and quantified using the NanoDrop ND-1000. RNA

samples were used for global m^6A expression profiling on an Arraystar Human

mRNA&lncRNA Epitranscriptomic Microarray (8 × 60 K; Arraystar), which includes

44,122 protein-coding mRNAs and 12,496 long non-coding RNAs. Microarray analyses

20

were entrusted to Arraystar Inc. (Rockville, MD, USA). Sample preparation and

microarray hybridization were performed based on Arraystar's standard protocols.

Briefly, total RNAs were immunoprecipitated with an anti-m^{6}A antibody (Synaptic

Systems, 202003). The "immunoprecipitated (IP)" and "supernatant (Sup)" RNAs were

labeled with Cy5 and Cy3, respectively, as cRNAs in separate reactions using the

Arraystar Super RNA Labeling Kit. The cRNAs were combined and hybridized onto

Arraystar Human mRNA&lncRNA Epitranscriptomic Microarray (8 $\times$ 60 K, Arraystar).

After washing the slides, the arrays were scanned in two-color channels using an

Agilent Scanner G2505C. Agilent Feature Extraction software (version 11.0.1.1) was

used to analyze acquired array images. Raw intensities of IP (Cy5-labeled) and Sup

(Cy3-labeled) were normalized with an average of log2-scaled Spike-in RNA intensities.

The "m^{6}A methylation level" was calculated to determine the percentage of

modification based on the IP (Cy5-labeled) and Sup (Cy3-labeled) normalized

intensities. "m^{6}A quantity" was calculated to determine the amount of m^{6}A methylation

based on the IP (Cy5-labeled) normalized intensities. Differentially m^{6}A-methylated

RNAs between both comparison groups were identified by filtering with a fold change

of >1.5 or <0.67 ($P < 0.01$) through the unpaired t-test. Microarray data had been

deposited in the GEO at the NCBI (accession number GSE165454).

21

qPCR for methylated RNA immunoprecipitation (MeRIP) with m⁶A antibody

ALKBH5-knockdown or control lung cancer cells were used for methylated RNA

immunoprecipitation assay. The Magna MeRIP m⁶A kit (catalog no.17-10499,

Millipore, Burlington, MA, USA) was used according to the manufacturer's protocol.

Briefly, the polyA-enriched RNA was fragmented into 100–200 nucleotides incubated

with RNA fragmentation buffer for 55 s (CS220011, Millipore). The size of

polyA-enriched RNA fragments was optimized using the Agilent 4200 TapeStation

(Agilent technologies, Santa Clara, CA, USA). We used 0.5 µg of fragmented

polyA-enriched RNA as input control and 5 µg of fragmented polyA-enriched RNA for

m⁶A mRNA immunoprecipitation, followed by incubation with m⁶A antibody

(MABE1006, Millipore)- or mouse IgG-conjugated Protein A/G Magnetic Beads in 500

µL 1× IP buffer supplemented with RNase inhibitors at 4□ overnight. Methylated

RNAs were immunoprecipitated with beads, eluted via competition with free m⁶A, and

purified using the RNeasy kit (Qiagen). Moreover, modification of m⁶A toward

particular genes was determined using qPCR analysis with specific primers [primers for

the positive control region (stop codon, EEF1A1+) or NC region (exon 5, EEF1A1−) of

human EEF1A1 was included in the Magna MeRIP m6A kit]. To design primers for

MeRIP qPCR, m^{6}A sites of specific genes were predicted using the sequence-based

RNA adenosine methylation site predictor algorithm (http://www.cuilab.cn/sramp) [55].

We focused on the potential m^{6}A sites in the 3′ UTRs near the stop codon and designed

primers to ensure that the target sequence were present in these sites with a limited

length of 120 nt. Self-designed primers for MeRIP qPCR are listed in Table S1.

Statistical analysis

Discrete variables were expressed as numbers (percentages), whereas continuous

variables were expressed as means ± standard deviations (SDs) unless otherwise

specified. The Mann–Whitney *U* test was used to compare continuous individual

samples, whereas Student's *t*-test was applied to compare continuous experimental data.

Fisher's exact test for independence was used to compare categorical data between

groups. The Wilcoxon matched-pairs signed-rank test was used to compare two

corresponding groups. Spearman's correlation coefficient was used for correlation

analysis. Kaplan–Meier curves with log-rank tests were used to analyze survival.

Accordingly, OS was defined as the duration from baseline to the date of death, whereas

recurrence-free survival (RFS) was defined as the duration from baseline to the

recurrence date. Univariate and multivariate Cox proportional hazards models were

23

applied to generate hazard ratios (HRs) for death while adjusting for other potential

confounding factors. Cell proliferation and RNA stability assays were analyzed using

two-way analysis of variance. Statistical analyses were performed using GraphPad

Prism Version 8 (GraphPad Software, San Diego, CA, USA) and EZR software

(Saitama Medical Center, Jichi Medical University, Saitama, Japan) [56], with P values

of <0.05 indicating statistical significance.

Results

High ALKBH5 expression was associated with a worse prognosis in patients with

NSCLC

To investigate the impact of ALKBH5 and FTO in NSCLC, we examined the mRNA

expression levels of ALKBH5 and FTO in non-cancerous lung tissues and NSCLC

tissues using TCGA data. Accordingly, our results showed no significant difference in

ALKBH5 mRNA expression between non-cancerous and cancerous tissues. By contrast,

our findings showed that NSCLC had a significantly lower FTO mRNA expression than

non-cancerous tissues (Figure 1a). We subsequently investigated the protein expression

levels of ALKBH5 and FTO in non-cancerous lung alveolar tissue and corresponding

NSCLC tissues using TMA of patient samples. Furthermore, our results showed that

24

cancerous tissues had significantly higher H-scores for ALKBH5 and FTO than non-cancerous tissues (Figure 1b). ALKBH5 and FTO expression were evaluated in immortalized bronchial epithelial cells (BEAS2B) and lung cancer cell lines. Consequently, qPCR analysis demonstrated that ALKBH5 mRNA expression was higher in lung cancer cell lines except LC-2/ad and RERF-LC–MS, whereas FTO mRNA expression was lower in lung cancer cell lines except HLC-1, ABC1, and PC3 (Figure 1c). Western blot analysis demonstrated that ALKBH5 and FTO were endogenously expressed in all lung cancer cell lines except HLC-1 (Figure 1d). IHC analysis showed that ALKBH5 and FTO were mainly localized in the nucleus of the cells (Figure 1e). Furthermore, immunofluorescence analysis showed that ALKBH5 was localized in the nucleus of PC9 cells overexpressing ALKBH5 (Figure 1f). We analyzed the clinical characteristics of 627 NSCLC cases used in IHC of TMA in the context of ALKBH5 or FTO expression in tumors of the HUSM cohort (Table 1). The median age was 68 (range, 23–88) years; 430 (68.6%) patients were male and 184 (29.3%) had never smoked. The tumors were histologically classified as adenocarcinoma (n = 413, 65.9%), squamous cell carcinoma (n = 170, 27.1%), or other histological types (n = 44, 7.0%). A total of 395 (63.0%) patients had stage I disease, whereas 127 (20.3%) cases had EGFR mutations. Postoperative adjuvant chemotherapy

25

was prescribed to 258 (41.1%) patients. The median H-score values for ALKBH5 and

FTO expression was 110 (0–225, range) and 65 (0–281), respectively, with high

ALKBH5 protein expression being correlated with high FTO protein expression (r =

0.41) (Figure S1A). Based on the median value, cases were divided into "high" and

"low" expression groups, after which their association with clinical data as well as

prognostic significance was examined. Lymph node metastasis, chemotherapy, and

EGFR status significantly differed depending on ALKBH5 expression, whereas tumor

status, lymph node metastasis, pathological stage, chemotherapy, and EGFR status

significantly differed depending on FTO expression. Kaplan–Meier curves showed that

patients with high ALKBH5 expression had significantly worse survival than those with

low ALKBH5 expression (Figure 1g: log-rank p = 0.0009 for OS; Figure S1B: log-rank

p = 0.0008 for RFS). Conversely, Kaplan–Meier curves showed no significant

difference in survival between the low and high FTO expression groups (Figure 1g:

log-rank p = 0.20 for OS, Figure S1C: log-rank p = 0.07 for RFS). Univariate analysis

revealed high ALKBH5 expression as a predictor of unfavorable OS (HR, 1.675; 95%

CI, 1.230–2.521). Moreover, multivariate analysis of age, sex, smoking status, histology,

pathological stage, and ALKBH5 expression revealed that ALKBH5 expression was an

independent prognostic factor associated with unfavorable OS (HR, 1.468; 95% CI,

26

1.039–2.073) (Table 2). To validate the prognostic value of ALKBH5 and FTO in other cohorts of patients with NSCLC, the lung cancer database in the Kaplan–Meier plotter was used. Accordingly, Kaplan–Meier curves showed that patients with high ALKBH5 expression had a significantly worse survival than those with low ALKBH5 expression (Figure S1D: log-rank p = 0.014 for OS). In contrast, Kaplan–Meier curves showed that patients with high FTO expression had significantly favorable survival compared with those with low FTO expression (log-rank p < 0.0001 for OS) (Figure S1E). These observations suggested that ALKBH5 played a critical role in the poor prognosis of patients with NSCLC.

ALKBH5 knockdown suppressed cell proliferation in NSCLC

To investigate the impact of ALKBH5 and FTO deficiency in lung cancer cell function, ALKBH5 and FTO were knocked down in PC9 and A549 cells using small interfering RNA (siRNA). Based on knockdown efficacy, ALKBH5 siRNA no. 1 (siALKBH5#1) and siRNA no. 3 (siALKBH5#3) and FTO siRNA no.1 (siFTO#1) and siRNA no. 3 (siFTO#3) were used in subsequent knockdown experiments (Figure 2a, 2b, and Figure S2A). ALKBH5 knockdown significantly suppressed the proliferation of PC9 and A549 cells (Figure 2c). By contrast, FTO knockdown showed no significant suppressive

effects on the proliferation of PC9 and A549 cells (Figure 2d). Thereafter, we assessed

migration abilities in ALKBH5-knockdown cells. Accordingly, the transwell migration

assay showed no significant reduction in the migratory PC9 and A549 cells (Figure 2e).

Moreover, the wound-healing assay showed that ALKBH5 knockdown promoted no

significant reduction in the migration ability of PC9 and A549 cells (Figure 2f, 2g).

Together with the prognostic value of ALKBH5 in NSCLC, these observations

suggested that ALKBH5 played a cancer-promoting role by regulating cell proliferation.

To subsequently examine the mechanism by which ALKBH5 knockdown

suppressed cell proliferation, cell cycle and apoptosis analyses were performed using

flow cytometry. Accordingly, ALKBH5 knockdown significantly increased the number

of PC9 cells in the G1 phase and reduced the number of PC9 cells in the G2/M phase

(Figure 3a, 3b). Conversely, ALKBH5 knockdown promoted no significant differences,

with a consistent result of two different sequences of siRNAs in the cell cycle of A549

(Figure3c, 3d). ALKBH5 knockdown increased the number of apoptotic PC9 cells

(Figure 3e, 3f). Furthermore, under drug-induced apoptosis via cisplatin and gefitinib

administration, ALKBH5 knockdown increased the number of apoptotic PC9 cells

(Figure 3g, 3h). ALKBH5 knockdown also increased the number of apoptotic A549

cells (Figure 3i, 3j). Moreover, ALKBH5 knockdown increased the number of apoptotic

28

A549 cells with cisplatin (Figure 3k, 3l). Overall, the aforementioned data showed that

ALKBH5 knockdown suppressed cell proliferation through G1 phase arrest and/or

apoptosis induction in NSCLC cell lines.

ALKBH5 overexpression promoted cell proliferation in immortalized cells

To analyze whether ALKBH5 overexpression in immortalized cells promoted malignant

changes in cell function, BEAS2B and HEK293 cells were infected with a

doxycycline-inducible vector, pRetroX-TetOne puro-ALKBH5. ALKBH5

overexpression was confirmed in HEK293 and BEAS2B cells (Figure 4a) and

significantly enhanced HEK293 and BEAS2B cell proliferation (Figure 4b and 4c). In

contrast, ALKBH5 overexpression showed no significant effects on the migration

ability of HEK293 (Figure 4d and 4e) and BEAS2B cells (Figure 4f and 4g). The

aforementioned results provided further evidence that ALKBH5 played a

cancer-promoting role by regulating cell proliferation.

ALKBH5 altered the abundance of m^{6}A modification in polyA-enriched RNA

To assess the amount of m^{6}A in cells, a quantitative evaluation of m^{6}A was performed

via LC–MS/MS using polyA-enriched RNA extracted from cells with altered ALKBH5

gene expression (Figure 5a). We investigated the technical variability that occurs when

adenosine and N^6-methyladenosine-d3 (m^{6}A-d3) are used as internal standards.

Although both adenosine (A) and m^{6}A-d3 showed a strong positive correlation with

m^{6}A (r = 0.92 and r = 0.90), the measurement with m^{6}A-d3 as the internal standard

showed less technical variability than that with A as the internal standard (Figure

S3A–C). Hence, we used m^{6}A-d3 as the internal control for subsequent experiments.

ALKBH5 knockdown increased m^{6}A modification in PC9 and A549 cells (Figure 5b

and 5C), whereas ALKBH5 overexpression reduced m^{6}A modification in a doxycycline

concentration-dependent manner in PC9 cells (Figure 5d, S3D, S3E). Moreover,

ALKBH5 overexpression reduced m^{6}A modification regardless of the time that had

elapsed after doxycycline addition (Figure 5e). Furthermore, ALKBH5 overexpression

reduced m^{6}A modification in BEAS2B and HEK293 cells (Figure 5f). The

aforementioned results presented evidence suggesting that ALKBH5 alters the global

m^{6}A abundance in cells.

ALKBH5 regulated the expression of cell proliferation-related genes

An expression microarray analysis was herein performed to investigate gene expression

profiles in ALKBH5-knockdown PC9 cells with two different sequences of siRNA

(ALKBH5#1 and ALKBH5#3). Differentially expressed genes (DEGs) were defined as those with a fold change of >1.5 or <0.67 ($P < 0.01$). A total of 697 DEGs were detected for ALKBH5#1 comprising 392 upregulated and 305 downregulated genes (Figure 6a), whereas 1394 DEGs were detected for ALKBH5#3 comprising 803 upregulated and 591 downregulated genes (Figure 6b). Moreover, 82 upregulated genes (Table S2) and 47 downregulated genes (Table S3) overlapped between ALKBH5#1 and ALKBH5#3 (Figure 6c). Except ALKBH5, genes associated with m^6A modification described in a previous review [57] were not included in the overlapped DEGs (Table S4). GSEA with the hallmark gene set revealed that the PC9 cells transfected with siALKBH5#1 and siALKBH5#3 had a more enriched expression of genes involved in cell cycle, such as MYC_TARGETS_V2, P53_PATHWAY, and G2/M_CHECKPOINT, than those transfected with siNC (Figure 6d and 6e). We selected 10 DEGs associated with cell proliferation bibliographically and confirmed the upregulation of E2F1, GADD45A, TIMP3, and CDKN1A and downregulation of CASP14 and CCNG2 by qPCR (Figure 6f). The aforementioned results revealed that ALKBH5 regulated the expression of genes associated with cell proliferation.

ALKBH5 altered the abundance of m6A in the 3′ UTR and regulated protein

expression of target genes

We performed m^6A-specific methylated RNA immunoprecipitation microarray analysis

in PC9 cells on an Arraystar Human mRNA&lncRNA Epitranscriptomic Microarray to

comprehensively examine whether differentially regulated genes were associated with

m^6A modification using unfragmented total RNA. The median methylation level in

unfragmented total RNA was 50.4% (6.8%–94.5%) (Figure S4A). A positive

correlation was observed between the methylation level in unfragmented total RNA and

the RNA length of each transcript (r = 0.35) (Figure S4B). Moreover, a negative

correlation was noted between the rate at which ALKBH5 knockdown increased m^6A

modification (methylation level in siALKBH5 − methylation level in siNC) and

methylation level at baseline (methylation level in siNC) (r = −0.35) (Figure S4C). The

volcano plot showed that 1 RNA was hypermethylated by ALKBH5#1 knockdown

(fold change > 1.5, $P < 0.01$) (Figure S4D), whereas 28 RNAs were hypermethylated by

ALKBH5#3 knockdown (fold change > 1.5; $P < 0.01$) (Figure S4E). No

hypermethylated genes overlapped between ALKBH5#1 and ALKBH5#3 knockdown

with a fold change threshold of >1.5 ($P < 0.01$) (Figure S4F). GSEA showed no

common hallmark gene set with an FDR q-value of < 0.25 for PC9 cells transfected

with siALKBH5#1 and siALKBH5#3 compared with the control group (Figure S4G).

Considering that the m6A levels of unfragmented RNAs regulated by ALKBH5

is affected by the baseline RNA length and endogenous m6A level, we performed

methylated RNA immunoprecipitation (MeRIP) with m^{6}A antibody using fragmented

polyA-enriched RNA in ALKBH5-knockdown PC9 cells to investigate focal m^{6}A

alterations in the mRNA. The fragmentation conditions were optimized (Figure S5A),

and the m^{6}A changes in the positive and NC were confirmed through qPCR using the

primers included in the Magna MeRIP m^{6}A Kit (Millipore) (Figure S5B). To verify the

accuracy of the MeRIP experiment, we selected MFAP5 out of the 11 genes that were

hypermethylated (>1.5 fold change and P < 0.05) in the human mRNA&lncRNA

Epitranscriptomic Microarray (Table S5) and analyzed the m^{6}A target site via qPCR.

Specific primers were designed for the predicted m^{6}A-harboring regions, and MeRIP

qPCR confirmed that ALKBH5 knockdown increased m^{6}A levels in the 3′ UTR of

MFAP5 (Figure S5C). Thereafter, MeRIP qPCR was performed in six DEGs verified

using qPCR with ALKBH5-knockdown PC9 cells. Our results showed increased m^{6}A

levels in the 3′ UTRs of CDKN1A, TIMP3, E2F1, and CCNG2 in

ALKBH5-knockdown PC9 cells (Figure 7a and Figure S5D). The aforementioned

33

results of the MeRIP qPCR suggest that ALKBH5 targeted the 3' UTRs of m^{6}A in these

four transcripts (Figure 7b).

Next, the protein expression levels of the potential target transcript of ALKBH5

were quantified by western blot analysis. Accordingly, our results showed that

CDKN1A (p21) expression increased independent of p53 in ALKBH5-knockdown PC9

cells, whereas TIMP3 expression increased in ALKBH5-knockdown A549 cells (Figure

7c).

IGF2BPs were required for ALKBH5 regulation of target mRNA expression via

stabilization of mRNA and affected cell proliferation

IGF2BP1, IGF2BP2, and IGF2BP3 (IGF2BPs) are well-known m^{6}A-recognizing

RNA-binding proteins and readers of m^{6}A that have been known to stabilize mRNA.

The expression of these proteins in a series of cell lines was analyzed by western

blotting, and the results showed significant differences in their expression in lung cancer

cells and immortalized bronchial epithelial cells according to the cell lines (Figure 8a).

Thereafter, ALKBH5 and IGF2BPs were knocked down with siRNA to

investigate the association between ALKBH5 and IGF2BPs and the expression of

CDKN1A or TIMP3 (Figure S6A, S6B, S6C, S6D, 8b). Accordingly, ALKBH5

knockdown increased the mRNA expressions of CDKN1A in PC9 cells (Figure 8c) and

TIMP3 in A549 cells (Figure 8d). In addition, the increased expression was offset by

the knockdown of IGF2BPs. Actinomycin D assay showed that ALKBH5 knockdown

stabilized CDKN1A mRNA in PC9 cells, and this stabilization was offset by the

knockdown of IGF2BPs (Figure 8e). ALKBH5 knockdown also stabilized TIMP3

mRNA in A549 cells, although not statistically significant, and this stabilization was

decreased by IGF2BP3 knockdown (Figure 8e). These results suggest that these

alterations in mRNA expression were offset by a double knockdown of both ALKBH5

and one of the IGF2BPs, and the decline of mRNAs were, at least partly, owing to the

destabilization of these mRNAs by one of the IGF2BPs. Additionally, we evaluated the

expression of ALKBH5 target mRNAs CDKN1A and TIMP3 in lung cancer using the

TCGA dataset. Accordingly, cancerous tissues (high ALKBH5 expression) had lower

CDKN1A and TIMP3 expression than non-cancerous tissue (low ALKBH5 expression)

(Figure S6E and S6F).

Considering that the interaction between ALKBH5 and IGF2BPs was found to

regulate the expression of genes associated with cell proliferation, cell proliferation

assays were conducted using ALKBH5- and IGF2BPs-knockdown cells. Notably,

ALKBH5 knockdown reduced cell proliferation in PC9 (Figure 8g) and A549 cells

35

(Figure 8h). The reduction of cell proliferation was offset by IGF2BPs knockdown.

These results support the hypothesis that IGF2BPs are required for ALKBH5 regulation

of target mRNA expression and cell proliferation.

Discussion

The current study revealed that ALKBH5 promoted poor survival and cell

proliferation in patients with NSCLC. Mechanistically, ALKBH5 knockdown had been

found to increase the expression of CDKN1A (p21) and TIMP3 by altering mRNA

stability in PC9 and A549 cells via m^6A change. Moreover, these changes in mRNA

stability were counteracted by IGF2BPs knockdown (particularly prominent in

IGF2BP3). The aforementioned results suggest that the recognition of target transcripts

by IGF2BPs stabilizes the mRNA of CDKN1A (p21) or TIMP3 and subsequently

increases their expressions, thereby regulating cell proliferation, cell cycle, and

apoptosis in lung cancer cell lines.

Over the last decade, considerable progression has been made on research

regarding the molecular mechanism for m^6A-mediated carcinogenesis of ALKBH5.

Nevertheless, previous studies on ALKBH5 have shown conflicting results regarding

the carcinogenic mechanisms of ALKBH5 across several cancers [31-39]. Two previous

studies have reported contradictory results regarding ALKBH5, suggesting that it acts

as either an oncogenic factor or a tumor suppressor in NSCLC [43, 44]. The current

study concluded that ALKBH5 exerted cancer-promoting effects in NSCLC by

suppressing CDKN1A (p21) or TIMP3. CDKN1A (p21) functions as a cell growth

suppressor by inhibiting cell cycle progression. Multiple transcription factors, ubiquitin

ligases, and protein kinases regulate the transcription, stability, and cellular localization

of CDKN1A (p21) [58]. A previous study showed that ALKBH5 knockdown increased

m^{6}A modification and mRNA stability of CDKN1A, which subsequently increased p21

protein expression and acted as a tumor suppressor in esophageal cancer [35]. Similarly,

our findings showed that ALKBH5 knockdown in PC9 cells acted as a tumor

suppressor by the upregulation of CDKN1A (p21) via m^{6}A alteration. We also showed

that p21 expression was p53-independent, indirectly reinforcing our finding that

CDKN1A (p21) upregulation was an m^{6}A-mediated response. Our results further

indicated a novel mechanism wherein changes in CDKN1A expression via ALKBH5

knockdown were rescued by IGF2BPs knockdown, which supports our finding that

alterations in CDKN1A (p21) expression were mediated by m^{6}A.

The current study identified TIMP3 as another important target molecule

downstream of ALKBH5. A previous study showed TIMP3 had several anticancer

37

properties, including apoptosis induction and antiproliferative, antiangiogenic, and antimetastatic activities. The expression of TIMP3 is regulated by transcription factors and histone acetylation [59]. Several studies have shown that TIMP3 acts as a tumor suppressor in lung cancer [60, 61]. Moreover, a previous report using A549 cell lines showed that ALKBH5 knockdown increases TIMP3 mRNA stability and TIMP3 expression via m^{6}A modification [44]. Similarly, the current study also confirmed that ALKBH5 knockdown increased mRNA stability, which increased TIMP3 protein expression, and acted as a tumor suppressor in A549 cells. Furthermore, our experimental data for the first time showed that the ALKBH5 knockdown-induced increase in TIMP3 was rescued by IGF2BPs, strongly suggesting that alterations in TIMP3 expression were mediated by m^{6}A.

Previous studies have reported that IGF2BPs, which are known as m^{6}A-recognizing RNA-binding proteins that stabilize m^{6}A-containing RNA, have oncogenic properties. Studies on lung cancer have associated IGF2BPs with cancer progression and poor prognosis [62-67]. Notably, a previous report showed that ALKBH5-mediated m^{6}A modification of LY6/PLAUR Domain Containing 1 (LYPD1) is recognized by IGF2BP1 and enhances the stability of LYPD1 mRNA in hepatocellular carcinoma [38]. Moreover, recent RNA-binding protein

38

immunoprecipitation-sequencing analysis using HEK293T showed that the binding site of IGF2BPs is mainly distributed in the 3′ UTRs and that the target of IGF2BPs preferentially binds to the consensus sequence of UGGAC in the target mRNA [29]. These findings support our experimental hypothesis that IGF2BPs recognize the m^{6}A in the 3′ UTRs of CDKN1A or TIMP3 because UGGAC is present within three locations in the 3′ UTRs of CDKN1A and two locations in the 3′ UTRs of TIMP3. Our findings also showed that the expression of IGF2BPs significantly differed with the lung cancer cell line, which can cause different fates of m^{6}A-modified transcripts among cell lines.

FTO inhibitors have been shown to suppress the progression of acute myeloid leukemia and glioblastoma *in vivo* [68, 69]. In contrast, the antitumor effects of ALKBH5 inhibitors, which enhanced the efficacy of cancer immunotherapy, have only been confirmed in melanomas [70]. Furthermore, several experimental facts have shown that ALKBH5 is associated with the malignant transformation of cancer [31-37], indicating that ALKBH5 inhibitors can be a target of tumor-agnostic therapy. However, it should be noted that ALKBH5 inhibitors may cause unexpected side effects in unknown target genes given that ALKBH5 inhibition alters the m6A modification of numerous transcripts and the expression of several genes.

Although the current study provided abundant evidence to conclude the remarkable role of the m^{6}A-regulated ALKBH5 and IGF2BPs axis in NSCLC, several limitations warrant consideration. First, given that RNAs were not fragmented during our epitranscriptomic microarray, site-specific changes in m^{6}A modification could not be determined. Considering the correlation between RNA length and ratio of m^{6}A-modified transcripts, the epitranscriptional micrarray analysis using unfragmented RNA does not allow the evaluation of multiple m6A modifications occurring within a single transcript. As such, we conducted MeRIP q-PCR with fragmented RNAs to evaluate site-specific differential m^{6}A modification. Nevertheless, the epitranscriptomic microarray with unfragmented RNAs provided a holistic view of the degree of m^{6}A modification for each transcript, establishing a landscape for m^{6}A modification by ALKBH5 knockdown (Figure S4A, S4B, S4C, S4D, S4E and S4G). Secondly, our epitranscriptomic microarray findings showed that ALKBH5-knockdown reduced m6A methylation levels in approximately half of the transcripts. Although the detailed mechanism remains unclear, hypomethylation may occur when some of the m^{6}A-rich transcripts bind to YTHDF2 and YTHDC2, reducing the stability of RNA containing m^{6}A. Consequently, the m^{6}A-modified transcript then undergoes degradation. In other words, the target's transcript may also differ depending on the elapsed time after the

perturbation of ALKBH5. However, the current study did not investigate the chronological alteration of the m^{6}A abundance of each transcript following ALKBH5 knockdown. Third, as mentioned earlier, CDKN1A and TIMP3 are also regulated by transcription factors or miRNA, and we cannot deny the possibility that mechanisms other than m^{6}A promoted changes in CDKN1A (p21) and TIMP3 expression. Nonetheless, the finding that IGF2BPs knockdown rescued the CDKN1A and TIMP3 expression supports our proposition that the changes in CDKN1A (p21) and TIMP3 expression were mediated by m^{6}A.

Conclusions

The current study revealed that increased ALKBH5 expression was an independent unfavorable prognostic factor in NSCLC. Moreover, upregulation of ALKBH5 in NSCLC reduced m^{6}A modifications on the 3' UTR of specific genes. The loss of m^{6}A decreased the opportunity for recognition by IGF2BPs and destabilized the target transcript, such as CDKN1A (p21) and TIMP3. Downregulation of CDKN1A (p21) and TIMP3 induced cell cycle alteration and inhibited apoptosis. Our results suggest that the ALKBH5–IGF2BPs axis promotes cell proliferation and tumorigenicity, which in turn causes the unfavorable prognosis of NSCLC. Our findings provide a novel insight into

41

the pathophysiological mechanisms of m^{6}A epitranscriptomic modification in NSCLC

(Figure 9). Further *in vivo* studies are nonetheless required to determine whether

ALKBH5 inhibitors can be incorporated in the treatment of NSCLC in the near future.

List of abbreviations

m^{6}A: N^6-methyladenosine; NSCLC: non-small cell lung cancer; MeRIP: Methylated

RNA immunoprecipitation; CI: Confidence interval; HR: Hazard ratio; UTRs: 3′

untranslated regions; METTL3: methyltransferase-like 3; METTL14:

Methyltransferase-like 14; WTAP: Wilms tumor 1-associated protein; RBM15:

RNA-binding motif protein 15; FTO: fat mass and obesity-related protein, ALKBH5:

AlkB homolog 5; YTHDC: YT521-B homology domain containing; HNRNPG:

heterogeneous nuclear ribonucleoprotein G; YTHDF: YT521-B homology domain

family; eIF3: eukaryotic initiation factor3; IGF2BP: insulin-like growth factor 2

mRNA-binding protein; m^{6}Am: N^6,2′-O-dimethyladenosine; TMA: Tissue microarray;

IHC: immunohistochemistry; TCGA: the Cancer Genome Atlas; RSEM: RNA-seq by

Expectation Maximization; DAPI: 4′,6-diamidino-2-phenylindole; siNC: siRNA

control; NT: non-treated cells; DOX: doxycycline; OE: overexpression; NC: negative

control; CCK-8: Cell Counting Kit-8; SDS: sodium dodecyl sulfate; PI: propidium

iodide; LC–MS/MS: liquid chromatography–mass spectrometry/mass spectrometry;

m^6A-d3: N^6-methyladenosine-d3; A: adenosine; FDR: false discovery rate; GSEA:

Gene set enrichment analysis; GEO: Gene Expression Omnibus; NCBI: National Center

for Biotechnology Information; SD: standard deviation; OS: Overall survival; RFS:

recurrence-free survival; ANOVA: analysis of variance; DEGs: differentially expressed

genes; LYPD1: LY6/PLAUR Domain Containing 1

Declarations

Acknowledgments

Author contributions

HS conceived this project, supervised all experiments and interpretations, and drafted

the manuscript. KT designed and performed all experiments, analyzed the data,

interpreted patient and experimental data, and drafted the manuscript. KY designed this project, performed sample collection, histological examination, and a part of the experiments and drafted the manuscript. Yusuke Inoue performed sample collection and histological examination. Yuji Iwashita designed this project, interpreted the experimental data, and drafted the manuscript. TO performed molecular experiments, interpreted the experimental data, and drafted the manuscript. HY and HW assisted part of the experiments. AK, MT, HO, and KF performed sample collection. KS performed sample collection and analyzed data. TS supervised this project. All authors have read and approved the final manuscript.

Funding

Availability of data and materials

All data and supplementary information within the article are available from the published article (including supplementary information files) or available on published

databases (TCGA or GEO). GEO accession numbers of our microarray data are GSE165453 and GSE165453.

Ethics approval and consent to participate

This study was approved by the Ethics Committees of Hamamatsu University School of Medicine (20-011) and Seirei Mikatahara General Hospital and was carried out in accordance with approved guidelines. Written informed consent was obtained from all patients. All analyses were conducted in compliance with the ethical standards according to the Helsinki Declaration.

Consent for publication

Not applicable.

Competing interests

The authors declare no competing interests.

Author details

1. Department of Tumor Pathology, Hamamatsu University School of Medicine,

Hamamatsu, Japan

2. Second Division, Department of Internal Medicine, Hamamatsu University

School of Medicine, Hamamatsu, Japan

3. Department of Physical Therapy, Faculty of Health and Medical Sciences, Tokoha

University, Hamamatsu, Japan

4. First Department of Surgery, Hamamatsu University School of Medicine,

Hamamatsu, Japan

5. Division of Thoracic Surgery, Respiratory Disease Center, Seirei Mikatahara

General Hospital, Hamamatsu, Japan

6. Department of Pathology, Seirei Mikatahara General Hospital, Hamamatsu, Japan

Figure legends

Figure 1. High ALKBH5 expression was associated with a worse prognosis in

patients with non-small cell lung cancer.

(**a**) ALKBH5 and FTO mRNA levels were analyzed in the paired non-cancerous and

NSCLC tissues using the TCGA database (n = 109 for each group). (**b**) ALKBH5 and

FTO protein levels were assessed in the paired non-cancerous lung alveolar tissue and NSCLC tissues in the HUSM cohort via immunohistochemistry (IHC) using the H-score (n = 77 for each group). (**c**) Relative ALKBH5 and FTO mRNA expression levels were detected using qPCR in cell lines. Data were normalized to GAPDH and adjusted to the expression of BEAS2B cells (ALKBH5: n = 4, FTO: n = 6). (**d**) ALKBH5 and FTO protein expression levels were determined using western blot analysis in cell lines. (**e**) IHC staining for ALKBH5 and FTO were assessed using the TMA core of NSCLC tissues in the HUSM cohort. Staining intensity was categorized into 0 (absent), 1 (weak), 2 (moderate), or 3 (strong). (**f**) Immunofluorescence visualized subcellular localization in PC9 cells (×100). PC9 cells infected with pRetroX-TetOne puro- ALKBH5 were transduced by 100 ng/mL of doxycycline and used as ALKBH5 overexpression. PC9 cells without doxycycline were used as a negative control. (**g**) A Kaplan–Meier survival curve with log-rank test was utilized to analyze the overall survival of the HUSM cohort. Patients were stratified into low (blue) or high expression groups (red) based on a cutoff determined by the median H-scores (n = 627). Results were presented as the median (a and b) or mean ± SD (c). ****$P <$ 0.0001 indicates a significant difference between the indicated groups.

Figure 2. ALKBH5 knockdown suppressed cell proliferation in non-small cell lung cancer

(**a, b**) Western blot analysis demonstrated ALKBH5 protein levels in cells transfected with siRNA for ALKBH5 (siALKBH5), FTO (siFTO), control (siNC), or non-treated cells (NT). (**c**) Cell proliferation relative to baseline in PC9 and A549 cells transfected with siALKBH5 (#1 and #3) or siNC were assessed using the CCK-8 assay (n = 3). (**d**) Cell proliferation relative to baseline in PC9 and A549 cells transfected with siFTO (#1 and #3) or siNC were assessed using the CCK-8 assay (n = 3). (**e**) Migration ability of PC9 and A549 cells transfected with siALKBH5 (#1 and #3) or siNC were assessed using transwell migration assay. The bar charts indicate the number of migratory cells that passed through the chamber membrane (n = 3). (**f, g**) Migration ability of PC9 (**f**) and A549 (**g**) cells transfected with siALKBH5 (#1 and #3) or siNC was assessed using wound-healing assay (n = 3). Results were presented as mean ± SD. $**P < 0.01$, $***P < 0.001$, $****P < 0.0001$ indicates a significant difference between the indicated groups.

Figure 3. ALKBH5 knockdown-induced G1 phase arrest of cell cycle and/or apoptosis in non-small cell lung cancer

48

(**a–d**) The cell cycle was examined via flow cytometry with PC9 (a) and A549 (c) cells

transfected with siALKBH5 (#1 and #3) or siNC. The bar charts indicate the percentage

of cells in each cell cycle phase [n = 6 for PC9 (b), n = 3 for A549 cells (d)]. (**e** and **f**)

Apoptotic cells were determined using flow cytometric analysis of PC9 cells transfected

with siALKBH5 (#1 and #3) or siNC. (e) Percentage of the apoptotic cells in which

both propidium iodide and Annexin V were positive are shown in a representative

scatter plot. (f) The apoptosis rate in ALKBH5 knockdown were compared with siNC

and shown as a bar chart (n = 3). (**g** and **h**) Cisplatin- or gefitinib-induced apoptotic

cells were determined via flow cytometry with PC9 cells transfected with siALKBH5 or

siNC. (g) Percentage of apoptotic cells shown in a representative scatter plot. (h) The

cisplatin- or gefitinib-induced apoptosis rate in ALKBH5 knockdown were compared

with siNC and shown as a bar chart (n = 3). (**i** and **j**) Apoptotic cells were determined

via flow cytometry with A549 cells transfected with siALKBH5 or siNC. (i) Percentage

of the apoptotic cells shown in a representative scatter plot. (j) Apoptosis rate in

ALKBH5 knockdown were compared with siNC and shown as a bar chart (n = 6). (**k**

and **l**) Cisplatin-induced apoptotic cells were determined via flow cytometric analysis of

A549 cells transfected with siALKBH5 or siNC. (k) Percentage of the apoptotic cells

shown in a representative scatter plot. (l) The cisplatin-induced apoptosis rate in

49

ALKBH5 knockdown were compared with siNC and shown as a bar chart (n = 3).

Results were presented as mean ± SD. *$P < 0.05$, **$P < 0.01$, ***$P < 0.001$, ****$P <$ 0.0001 indicates a significant difference between the indicated groups.

Figure 4. ALKBH5 overexpression promoted cell proliferation

Immortalized cells infected with pRetroX-TetOne puro empty vector (empty) or

pRetroX-TetOne puro-ALKBH5 (ALKBH5) were used to assess the function of

ALKBH5-overexpressed cells. The concentration of doxycycline (DOX) was 100

ng/mL. (**a**) Western blot analysis demonstrated ALKBH5 protein levels in

ALKBH5-overexpressed HEK293 and BEAS2B cells. (**b, c**) Cells infected with

pRetroX-TetOne puro-ALKBH5 with DOX were designated as ALKBH5

overexpression (OE), whereas those without DOX were designated as negative control

(NC). Cell proliferation relative to baseline in ALKBH5 OE HEK293 and BEAS2B

cells were assessed using the CCK-8 assay (n = 3). (**d–g**) The migration ability of

HEK293 and BEAS2B cells was assessed via wound-healing assay. Representative

images of the wound-healing assay for HEK293 (**d**) and BEAS2B (**f**) cells. Wound

areas relative to baseline at each time point were compared between ALKBH5 OE and

50

NC HEK293 (**e**) and BEAS2B (**g**) cells (n = 3). Results are presented as mean ± SD. *P*

< 0.05 indicates a significant difference between the indicated groups.

Figure 5. ALKBH5 altered the abundance of m^{6}A modification in polyA-enriched RNA

(**a**) Representative chromatograms obtained using liquid chromatography–mass

spectrometry/mass spectrometry (LC–MS/MS) for adenosine (upper panel, 2.89 min),

N^6-methyladenosine (middle panel, 3.81 min), and N^6-methyladenosine-d3 (lower panel,

3.76 min) in polyA-enriched RNA extracted from PC9 cells. Peak areas were quantified

as the product of retention time (min) and count per seconds (cps). (**b** and **c**) The peak

areas of m^{6}A were normalized to that of m6A-d3. The amount of m^{6}A in PC9 (b) and

A549 (c) cells transfected with siALKBH5 were compared with that in cells transfected

with siNC for 48, 72, and 96 h (n = 3). (**d**) PolyA-enriched RNAs were extracted from

PC9 cells containing pRetroX-TetOne puro-ALKBH5 vector. m^{6}A/m^{6}A-d3 in the cells

incubated with various concentrations of DOX for 48 h were compared with that in cells

incubated with 0 ng/mL DOX (n = 3). (**e**) m^{6}A/m^{6}A-d3 in PC9 cells containing

pRetroX-TetOne puro-ALKBH5 vector (ALKBH5 OE) whose ALKBH5

overexpression was induced by 100 ng/mL DOX for 24, 48, 72, 96, 120 h was

51

compared with those without DOX (NC) (n = 3). (**f**) m^6A/m^6A-d3 in HEK293 and

BEAS2B (ALKBH5 OE) cells whose ALKBH5 overexpression was induced by 100

ng/mL DOX for 48 h were compared with those without DOX (NC) (n = 3). Results

were presented as mean ± SD. *$P < 0.05$, **$P < 0.01$, ***$P < 0.001$, ****$P < 0.0001$

indicates a significant difference between the indicated groups by Student's t-test.

Figure 6. ALKBH5 knockdown regulated cell proliferation-related genes

PC9 cells were transfected with siNC, siALKBH5#1, or siALKBH5#3 for 96 h (n = 3

for each group). (**a, b**) Differentially expressed genes (DEGs) for siALKBH5#1 (a) or

siALKBH5#3 (b) were detected using expression microarray and shown using volcano

plots. Dashed lines indicate the threshold for the differential expression [fold change >

1.5 (log2 fold change = 0.5849) or < 0.67 (log2 fold change = −0.5849), $P < 0.01$ via

Student's t-test] for upregulated (pink dots) or downregulated (light blue dots) genes. (**c**)

Venn diagram indicating the number of common DEGs in ALKBH5-knockdown cells

with different siRNA sequences. (**d**) Expression profiles of PC9 cells transfected with

siALKBH5#1 (in the left panel) and siALKBH5#3 (in the right panel) were compared

with those transfected with siNC via gene set enrichment analysis using hallmark gene

sets. Significantly enriched gene sets were defined as those with FDR of < 0.25.

52

Common enrichment gene sets between PC9 cells transfected with siALKBH5#1 and

siALKBH5#3 were listed in the right panel. (**e**) The ranks of genes involved in

MYC_TARGETS_V2, P53_PATHWAY, and G2/M_CHECKPOINT (black vertical

bars) are enriched in highly upregulated genes through both ALKBH5#1(left side) and

ALKBH5 #3 (right side) knockdown (red side). (**f**) mRNA expression levels of genes

related to cell proliferation in ALKBH5-knockdown PC9 cells were analyzed using

qPCR. Gene expression was normalized to the GAPDH expression and was shown

relative to the expression with siNC. Results are presented as mean $\pm$ SD. *$P < 0.05$,

**$P < 0.01$, ***$P < 0.001$, ****$P < 0.0001$ indicates a significant difference between

the indicated groups.

Figure 7. ALKBH5 altered m^{6}A abundance in the 3′ untranslated regions of

specific genes and protein expression

(**a**) m^{6}A level in the 3′ UTRs of target mRNA in PC9 cells transfected with

siALKBH5#1 or siALKBH5#3 was quantified via MeRIP qPCR using anti-m6A

antibody and was compared with that in cell transfected with siNC. The m^{6}A level was

normalized to that of input fraction (n = 3). IgG was used to evaluate the non-specific

binding of the target mRNA. (**b**) A schematic outline showing the workflow for the

analysis of downstream targets of ALKBH5. (**c**) Target protein levels in PC9 or A549

cells transfected with siALKBH5#1 or siALKBH5#3 were compared with those

transfected with siNC via western blot analysis. Results are presented as mean ± SD. *P

< 0.05, **P < 0.01, ***P < 0.001, ****P < 0.0001 indicates a significant difference

between the indicated groups.

Figure 8. IGF2BPs was required for the ALKBH5-induced regulation of mRNA

expression and cell proliferation

(**a**) Expression levels of IGF2BP1, IGF2BP2, and IGF2BP3 (IGF2BPs) protein

determined using western blot analysis were compared between cell lines. (**b**) IGF2BP

protein levels in cells transfected with siALKBH5 (left end), those in cells transfected

with siIGF2BP1, siIGF2BP2, or siIGF2BP3 with or without siALKBH5 (middle two

lanes), or those with siNC (right end indicating both siALKBH5 and siIGF2BPs were

negative) were confirmed via western blot analysis. (**c** and **d**) Endogenous mRNA

expression levels of CDKN1A in PC9 cells (c) or those of TIMP3 in A549 cells (d)

transfected with siALKBH5 were analyzed via qPCR and compared with those in cells

co-transfected with siALKBH5 and one of the siIGF2BPs. Gene expression was

normalized to the GAPDH expression and was shown relative to the expression in siNC

(n = 3). (**d** and **e**) The remaining RNA level of CDKN1A in PC9 cells (d) or of TIMP3

in A549 cells (e) after actinomysin D treatment for 0, 2, 4, and 6 h was determined

using qPCR and normalized to the expression at 0 h. RNA decay rate in cells

transfected with siALKBH5 and/or one of the siIGF2BPs and siNC were compared with

the stability of CDKN1A and TIMPs (n = 3). (**g** and **h**) Cell proliferation relative to

baseline in PC9 (e) and A549 (f) cells transfected with siALKBH5 was assessed via the

CCK-8 assay and compared with that in cells cotransfected with siALKBH5 and one of

the siIGF2BPs (n = 3 for each group). Results are presented as mean ± SD. *$P < 0.05$,

**$P < 0.01$, ***$P < 0.001$, ****$P < 0.0001$ indicates a significant difference between

the indicated groups.

Figure 9. Schematic illustration for the proposed mechanism of tumorigenicity via

ALKBH5 in non-small cell lung cancer

Upregulation of ALKBH5 in NSCLC reduces m^{6}A modifications on the 3′ UTR of

specific genes. The loss of m^{6}A decreases the opportunity for recognition by IGF2BPs

and destabilizes the target transcript, such as CDKN1A (p21) and TIMP3.

Downregulation of CDKN1A (p21) and TIMP3 induces cell cycle alteration and

inhibits apoptosis. This ALKBH5–IGF2BPs axis promotes cell proliferation and

tumorigenicity, which in turn causes the unfavorable prognosis of NSCLC.

References

1. WHO report on cancer: setting priorities, investing wisely and providing care for all [https://www.who.int/publications/i/item/who-report-on-cancer-setting-priorities-investing-wisely-and-providing-care-for-all]

2. Mok TS, Wu YL, Thongprasert S, Yang CH, Chu DT, Saijo N, Sunpaweravong P, Han B, Margono B, Ichinose Y, et al: Gefitinib or carboplatin-paclitaxel in pulmonary adenocarcinoma. *N Engl J Med* 2009, 361:947-957.

3. Shaw AT, Kim DW, Nakagawa K, Seto T, Crino L, Ahn MJ, De Pas T, Besse B, Solomon BJ, Blackhall F, et al: Crizotinib versus chemotherapy in advanced ALK-positive lung cancer. *N Engl J Med* 2013, 368:2385-2394.

4. Planchard D, Besse B, Groen HJM, Souquet P-J, Quoix E, Baik CS, Barlesi F, Kim TM, Mazieres J, Novello S, et al: Dabrafenib plus trametinib in patients with previously treated BRAFV600E-mutant metastatic non-small cell lung cancer: an open-label, multicentre phase 2 trial. *The Lancet Oncology* 2016, 17:984-993.

5.   Shaw AT, Ou SH, Bang YJ, Camidge DR, Solomon BJ, Salgia R, Riely GJ, Varella-Garcia M,

      Shapiro GI, Costa DB, et al: Crizotinib in ROS1-rearranged non-small-cell lung cancer. *N Engl J*

      Med 2014, 371:1963-1971.

6.   Gandhi L, Rodriguez-Abreu D, Gadgeel S, Esteban E, Felip E, De Angelis F, Domine M,

      Clingan P, Hochmair MJ, Powell SF, et al: Pembrolizumab plus Chemotherapy in Metastatic

      Non-Small-Cell Lung Cancer. *N Engl J Med* 2018, 378:2078-2092.

7.   Carroll SM, Narayan P, Rottman FM: N6-methyladenosine residues in an intron-specific region

      of prolactin pre-mRNA. *Mol Cell Biol* 1990, 10:4456-4465.

8.   Dominissini D, Moshitch-Moshkovitz S, Schwartz S, Salmon-Divon M, Ungar L, Osenberg S,

      Cesarkas K, Jacob-Hirsch J, Amariglio N, Kupiec M, et al: Topology of the human and mouse

      m6A RNA methylomes revealed by m6A-seq. *Nature* 2012, 485:201-206.

9.   Liu J, Yue Y, Han D, Wang X, Fu Y, Zhang L, Jia G, Yu M, Lu Z, Deng X, et al: A

      METTL3-METTL14 complex mediates mammalian nuclear RNA N6-adenosine methylation.

      Nat Chem Biol 2014, 10:93-95.

10.   Ping XL, Sun BF, Wang L, Xiao W, Yang X, Wang WJ, Adhikari S, Shi Y, Lv Y, Chen YS, et

      al: Mammalian WTAP is a regulatory subunit of the RNA N6-methyladenosine

      methyltransferase. *Cell Research* 2014, 24:177-189.

11.   Yue Y, Liu J, Cui X, Cao J, Luo G, Zhang Z, Cheng T, Gao M, Shu X, Ma H, et al: VIRMA

      mediates preferential m(6)A mRNA methylation in 3'UTR and near stop codon and associates

      with alternative polyadenylation. *Cell Discov* 2018, 4:10.

12.   Patil DP, Chen CK, Pickering BF, Chow A, Jackson C, Guttman M, Jaffrey SR: m(6)A RNA

      methylation promotes XIST-mediated transcriptional repression. *Nature* 2016, 537:369-373.

13.   Jia G, Fu Y, Zhao X, Dai Q, Zheng G, Yang Y, Yi C, Lindahl T, Pan T, Yang YG, He C:

      N6-methyladenosine in nuclear RNA is a major substrate of the obesity-associated FTO. *Nat*

      Chem Biol 2011, 7:885-887.

14.   Zheng G, Dahl JA, Niu Y, Fedorcsak P, Huang CM, Li CJ, Vagbo CB, Shi Y, Wang WL, Song

      SH, et al: ALKBH5 is a mammalian RNA demethylase that impacts RNA metabolism and

      mouse fertility. *Mol Cell* 2013, 49:18-29.

15.   Mauer J, Luo X, Blanjoie A, Jiao X, Grozhik AV, Patil DP, Linder B, Pickering BF, Vasseur JJ,

      Chen Q, et al: Reversible methylation of m(6)Am in the 5' cap controls mRNA stability. *Nature*

      2017, 541:371-375.

16.   Meyer KD, Saletore Y, Zumbo P, Elemento O, Mason CE, Jaffrey SR: Comprehensive analysis

      of mRNA methylation reveals enrichment in 3' UTRs and near stop codons. *Cell* 2012,

      149:1635-1646.

17.   Tang C, Klukovich R, Peng H, Wang Z, Yu T, Zhang Y, Zheng H, Klungland A, Yan W:

ALKBH5-dependent m6A demethylation controls splicing and stability of long 3'-UTR mRNAs

in male germ cells. *Proc Natl Acad Sci U S A* 2018, 115:E325-E333.

18.   Xiao W, Adhikari S, Dahal U, Chen YS, Hao YJ, Sun BF, Sun HY, Li A, Ping XL, Lai WY, et

al: Nuclear m(6)A Reader YTHDC1 Regulates mRNA Splicing. *Mol Cell* 2016, 61:507-519.

19.   Haussmann IU, Bodi Z, Sanchez-Moran E, Mongan NP, Archer N, Fray RG, Soller M: m(6)A

potentiates Sxl alternative pre-mRNA splicing for robust Drosophila sex determination. *Nature*

2016, 540:301-304.

20.   Zhao X, Yang Y, Sun BF, Shi Y, Yang X, Xiao W, Hao YJ, Ping XL, Chen YS, Wang WJ, et al:

FTO-dependent demethylation of N6-methyladenosine regulates mRNA splicing and is required

for adipogenesis. *Cell Res* 2014, 24:1403-1419.

21.   Roundtree IA, Luo GZ, Zhang Z, Wang X, Zhou T, Cui Y, Sha J, Huang X, Guerrero L, Xie P,

et al: YTHDC1 mediates nuclear export of N(6)-methyladenosine methylated mRNAs. *Elife*

2017, 6.

22.   Liu N, Dai Q, Zheng G, He C, Parisien M, Pan T: N(6)-methyladenosine-dependent RNA

structural switches regulate RNA-protein interactions. *Nature* 2015, 518:560-564.

23. Liu N, Zhou KI, Parisien M, Dai Q, Diatchenko L, Pan T: N6-methyladenosine alters RNA structure to regulate binding of a low-complexity protein. *Nucleic Acids Res* 2017, 45:6051-6063.

24. Li A, Chen YS, Ping XL, Yang X, Xiao W, Yang Y, Sun HY, Zhu Q, Baidya P, Wang X, et al: Cytoplasmic m(6)A reader YTHDF3 promotes mRNA translation. *Cell Res* 2017, 27:444-447.

25. Choe J, Lin S, Zhang W, Liu Q, Wang L, Ramirez-Moya J, Du P, Kim W, Tang S, Sliz P, et al: mRNA circularization by METTL3-eIF3h enhances translation and promotes oncogenesis. *Nature* 2018, 561:556-560.

26. Wang X, Zhao BS, Roundtree IA, Lu Z, Han D, Ma H, Weng X, Chen K, Shi H, He C: N(6)-methyladenosine Modulates Messenger RNA Translation Efficiency. *Cell* 2015, 161:1388-1399.

27. Shi H, Wang X, Lu Z, Zhao BS, Ma H, Hsu PJ, Liu C, He C: YTHDF3 facilitates translation and decay of N(6)-methyladenosine-modified RNA. *Cell Res* 2017, 27:315-328.

28. Wang X, Lu Z, Gomez A, Hon GC, Yue Y, Han D, Fu Y, Parisien M, Dai Q, Jia G, et al: N6-methyladenosine-dependent regulation of messenger RNA stability. *Nature* 2014, 505:117-120.

29.   Huang H, Weng H, Sun W, Qin X, Shi H, Wu H, Zhao BS, Mesquita A, Liu C, Yuan CL, et al:

        Recognition of RNA N(6)-methyladenosine by IGF2BP proteins enhances mRNA stability and

        translation. *Nat Cell Biol* 2018, 20:285-295.

30.   Ma L, Chen T, Zhang X, Miao Y, Tian X, Yu K, Xu X, Niu Y, Guo S, Zhang C, et al: The

        m(6)A reader YTHDC2 inhibits lung adenocarcinoma tumorigenesis by suppressing

        SLC7A11-dependent antioxidant function. *Redox Biol* 2021, 38:101801.

31.   Zhang S, Zhao BS, Zhou A, Lin K, Zheng S, Lu Z, Chen Y, Sulman EP, Xie K, Bogler O, et al:

        m(6)A Demethylase ALKBH5 Maintains Tumorigenicity of Glioblastoma Stem-like Cells by

        Sustaining FOXM1 Expression and Cell Proliferation Program. *Cancer Cell* 2017, 31:591-606

        e596.

32.   Chen S, Zhou L, Wang Y: ALKBH5-mediated m(6)A demethylation of lncRNA PVT1 plays an

        oncogenic role in osteosarcoma. *Cancer Cell Int* 2020, 20:34.

33.   Guo T, Liu DF, Peng SH, Xu AM: ALKBH5 promotes colon cancer progression by decreasing

        methylation of the lncRNA NEAT1. *Am J Transl Res* 2020, 12:4542-4549.

34.   Jiang Y, Wan Y, Gong M, Zhou S, Qiu J, Cheng W: RNA demethylase ALKBH5 promotes

        ovarian carcinogenesis in a simulated tumour microenvironment through stimulating NF-kappaB

        pathway. *J Cell Mol Med* 2020, 24:6137-6148.

35.   Nagaki Y, Motoyama S, Yamaguchi T, Hoshizaki M, Sato Y, Sato T, Koizumi Y, Wakita A, Kawakita Y, Imai K, et al: m(6) A demethylase ALKBH5 promotes proliferation of esophageal squamous cell carcinoma associated with poor prognosis. *Genes Cells* 2020, 25:547-561.

36.   Pu X, Gu Z, Gu Z: ALKBH5 regulates IGF1R expression to promote the Proliferation and Tumorigenicity of Endometrial Cancer. *J Cancer* 2020, 11:5612-5622.

37.   Zhang X, Wang F, Wang Z, Yang X, Yu H, Si S, Lu J, Zhou Z, Lu Q, Wang Z, Yang H: ALKBH5 promotes the proliferation of renal cell carcinoma by regulating AURKB expression in an m(6)A-dependent manner. *Ann Transl Med* 2020, 8:646.

38.   Chen Y, Zhao Y, Chen J, Peng C, Zhang Y, Tong R, Cheng Q, Yang B, Feng X, Lu Y, et al: ALKBH5 suppresses malignancy of hepatocellular carcinoma via m(6)A-guided epigenetic inhibition of LYPD1. *Mol Cancer* 2020, 19:123.

39.   Guo X, Li K, Jiang W, Hu Y, Xiao W, Huang Y, Feng Y, Pan Q, Wan R: RNA demethylase ALKBH5 prevents pancreatic cancer progression by posttranscriptional activation of PER1 in an m6A-YTHDF2-dependent manner. *Mol Cancer* 2020, 19:91.

40.   Liu J, Ren D, Du Z, Wang H, Zhang H, Jin Y: m(6)A demethylase FTO facilitates tumor progression in lung squamous cell carcinoma by regulating MZF1 expression. *Biochem Biophys Res Commun* 2018, 502:456-464.

41.   Li J, Han Y, Zhang H, Qian Z, Jia W, Gao Y, Zheng H, Li B: The m6A demethylase FTO

        promotes the growth of lung cancer cells by regulating the m6A level of USP7 mRNA. *Biochem*

        Biophys Res Commun 2019, 512:479-485.

42.   Ding Y, Qi N, Wang K, Huang Y, Liao J, Wang H, Tan A, Liu L, Zhang Z, Li J, et al: FTO

        Facilitates Lung Adenocarcinoma Cell Progression by Activating Cell Migration Through

        mRNA Demethylation. *Onco Targets Ther* 2020, 13:1461-1470.

43.   Jin D, Guo J, Wu Y, Yang L, Wang X, Du J, Dai J, Chen W, Gong K, Miao S, et al: m(6)A

        demethylase ALKBH5 inhibits tumor growth and metastasis by reducing YTHDFs-mediated

        YAP expression and inhibiting miR-107/LATS2-mediated YAP activity in NSCLC. *Mol Cancer*

        2020, 19:40.

44.   Zhu Z, Qian Q, Zhao X, Ma L, Chen P: N(6)-methyladenosine ALKBH5 promotes non-small

        cell lung cancer progress by regulating TIMP3 stability. *Gene* 2020, 731:144348.

45.   Zhang C, Samanta D, Lu H, Bullen JW, Zhang H, Chen I, He X, Semenza GL: Hypoxia induces

        the breast cancer stem cell phenotype by HIF-dependent and ALKBH5-mediated

        m(6)A-demethylation of NANOG mRNA. *Proc Natl Acad Sci U S A* 2016, 113:E2047-2056.

46.   Chao Y, Shang J, Ji W: ALKBH5-m(6)A-FOXM1 signaling axis promotes proliferation and

        invasion of lung adenocarcinoma cells under intermittent hypoxia. *Biochem Biophys Res*

        Commun 2020, 521:499-506.

47. Inoue Y, Matsuura S, Kurabe N, Kahyo T, Mori H, Kawase A, Karayama M, Inui N, Funai K, Shinmura K, et al: Clinicopathological and Survival Analysis of Japanese Patients with Resected Non-Small-Cell Lung Cancer Harboring NKX2-1, SETDB1, MET, HER2, SOX2, FGFR1, or PIK3CA Gene Amplification. *Journal of Thoracic Oncology* 2015, 10:1590-1600.

48. Inoue Y, Yoshimura K, Kurabe N, Kahyo T, Kawase A, Tanahashi M, Ogawa H, Inui N, Funai K, Shinmura K, et al: Prognostic impact of CD73 and A2A adenosine receptor expression in non-small-cell lung cancer. *Oncotarget* 2017, 8:8738-8751.

49. Matsuura S, Kahyo T, Shinmura K, Iwaizumi M, Yamada H, Funai K, Kobayashi J, Tanahashi M, Niwa H, Ogawa H, et al: SGOL1 variant B induces abnormal mitosis and resistance to taxane in non-small cell lung cancers. *Sci Rep* 2013, 3:3012.

50. Sugimura: Secreted form of EphA7 in lung cancer. *International Journal of Oncology* 2010, 36.

51. Collins TJ: ImageJ for microscopy. *Biotechniques* 2007, 43:25-30.

52. Horiuchi K, Umetani M, Minami T, Okayama H, Takada S, Yamamoto M, Aburatani H, Reid PC, Housman DE, Hamakubo T, Kodama T: Wilms' tumor 1-associating protein regulates G2/M transition through stabilization of cyclin A2 mRNA. *Proc Natl Acad Sci U S A* 2006, 103:17278-17283.

53. Du C, Kurabe N, Matsushima Y, Suzuki M, Kahyo T, Ohnishi I, Tanioka F, Tajima S, Goto M, Yamada H, et al: Robust quantitative assessments of cytosine modifications and changes in the expressions of related enzymes in gastric cancer. *Gastric Cancer* 2015, 18:516-525.

54. Subramanian A, Tamayo P, Mootha VK, Mukherjee S, Ebert BL, Gillette MA, Paulovich A, Pomeroy SL, Golub TR, Lander ES, Mesirov JP: Gene set enrichment analysis: a knowledge-based approach for interpreting genome-wide expression profiles. *Proc Natl Acad Sci U S A* 2005, 102:15545-15550.

55. Zhou Y, Zeng P, Li YH, Zhang Z, Cui Q: SRAMP: prediction of mammalian N6-methyladenosine (m6A) sites based on sequence-derived features. *Nucleic Acids Res* 2016, 44:e91.

56. Kanda Y: Investigation of the freely available easy-to-use software 'EZR' for medical statistics. *Bone Marrow Transplant* 2013, 48:452-458.

57. Zhou Z, Lv J, Yu H, Han J, Yang X, Feng D, Wu Q, Yuan B, Lu Q, Yang H: Mechanism of RNA modification N6-methyladenosine in human cancer. *Mol Cancer* 2020, 19:104.

58. Abbas T, Dutta A: p21 in cancer: intricate networks and multiple activities. *Nat Rev Cancer* 2009, 9:400-414.

59. Su CW, Lin CW, Yang WE, Yang SF: TIMP-3 as a therapeutic target for cancer. *Ther Adv Med Oncol* 2019, 11:1758835919864247.

60. Lei Y, Liu Z, Yang W: Negative correlation of cytoplasm TIMP3 with miR-222 indicates a good prognosis for NSCLC. *Onco Targets Ther* 2018, 11:5551-5557.

61. Garofalo M, Di Leva G, Romano G, Nuovo G, Suh SS, Ngankeu A, Taccioli C, Pichiorri F, Alder H, Secchiero P, et al: miR-221&222 regulate TRAIL resistance and enhance tumorigenicity through PTEN and TIMP3 downregulation. *Cancer Cell* 2009, 16:498-509.

62. Huang X, Zhang H, Guo X, Zhu Z, Cai H, Kong X: Insulin-like growth factor 2 mRNA-binding protein 1 (IGF2BP1) in cancer. *J Hematol Oncol* 2018, 11:88.

63. Kato T, Hayama S, Yamabuki T, Ishikawa N, Miyamoto M, Ito T, Tsuchiya E, Kondo S, Nakamura Y, Daigo Y: Increased expression of insulin-like growth factor-II messenger RNA-binding protein 1 is associated with tumor progression in patients with lung cancer. *Clin Cancer Res* 2007, 13:434-442.

64. Huang RS, Zheng YL, Li C, Ding C, Xu C, Zhao J: MicroRNA-485-5p suppresses growth and metastasis in non-small cell lung cancer cells by targeting IGF2BP2. *Life Sci* 2018, 199:104-111.

65. Findeis-Hosey JJ, Yang Q, Spaulding BO, Wang HL, Xu H: IMP3 expression is correlated with histologic grade of lung adenocarcinoma. *Hum Pathol* 2010, 41:477-484.

66. Findeis-Hosey JJ, Xu H: Insulin-like growth factor II-messenger RNA-binding protein-3 and lung cancer. *Biotech Histochem* 2012, 87:24-29.

67.   Zhao W, Lu D, Liu L, Cai J, Zhou Y, Yang Y, Zhang Y, Zhang J: Insulin-like growth factor 2

        mRNA binding protein 3 (IGF2BP3) promotes lung tumorigenesis via attenuating p53 stability.

        Oncotarget 2017, 8:93672-93687.

68.   Cui Q, Shi H, Ye P, Li L, Qu Q, Sun G, Sun G, Lu Z, Huang Y, Yang CG, et al: m(6)A RNA

        Methylation Regulates the Self-Renewal and Tumorigenesis of Glioblastoma Stem Cells. *Cell*

        Rep 2017, 18:2622-2634.

69.   Huang Y, Su R, Sheng Y, Dong L, Dong Z, Xu H, Ni T, Zhang ZS, Zhang T, Li C, et al:

        Small-Molecule Targeting of Oncogenic FTO Demethylase in Acute Myeloid Leukemia. *Cancer*

        Cell 2019, 35:677-691 e610.

70.   Li N, Kang Y, Wang L, Huff S, Tang R, Hui H, Agrawal K, Gonzalez GM, Wang Y, Patel SP,

        Rana TM: ALKBH5 regulates anti-PD-1 therapy response by modulating lactate and suppressive

        immune cell accumulation in tumor microenvironment. *Proc Natl Acad Sci U S A* 2020,

        117:20159-20170.
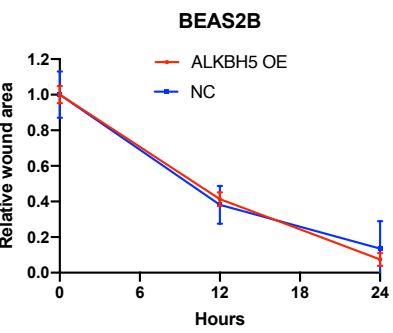
Figure 1
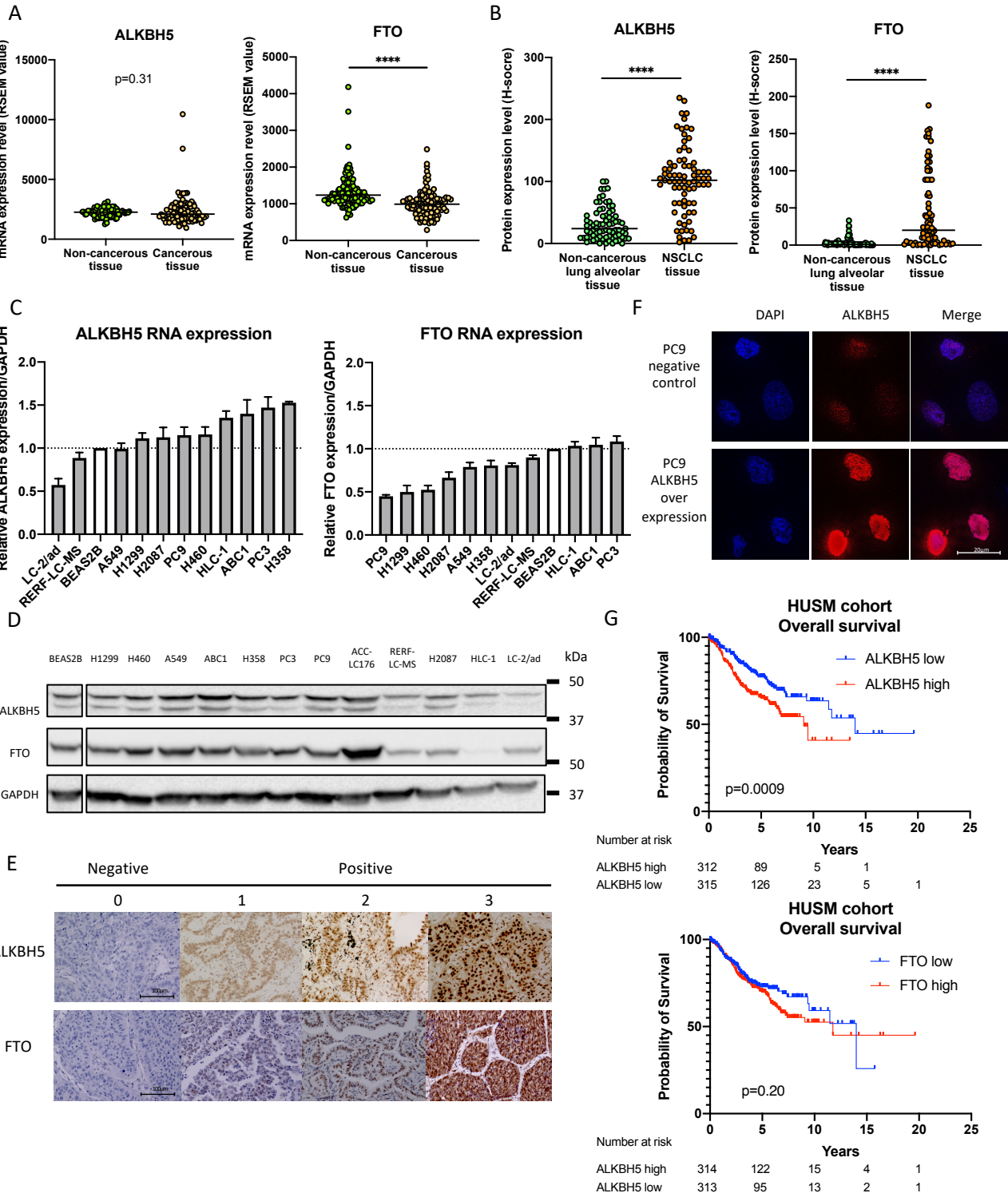
Figure 2

Figure 3

Figure 4

A

B

HEK293

C

BEAS2B

D

HEK293

F

BEAS2B

E

HEK293

G

BEAS2B

Figure 5

Figure 6

A

siALKBH5#1

Downregulated
305 genes

Upregulated
392 genes

B

siALKBH5#3

Downregulated
591 genes

Upregulated
803 genes

C

Upregulated genes

siALKBH5#1   siALKBH5#3

392 **82** 803

Downregulated genes

siALKBH5#1   siALKBH5#3

305 **47** 591

D

siALKBH5#1

Hallmark gene sets

**Common enrichment gene sets
between siALKBH5#1 and siALKBH5#3**

ANGIOGENESIS
APOPTOSIS
EPITHELIAL_MESENCHYMAL_TRANSITION
ESTROGEN_RESPONSE_EARLY
G2M_CHECKPOINT
HYPOXIA
KRAS_SIGNALING_UP
MYC_TARGETS_V2
P53_PATHWAY
TNFA_SIGNALING_VIA_NFKB
UNFOLDED_PROTEIN_RESPONSE
UV_RESPONSE_UP

siALKBH5#3

Hallmark gene sets

E

siALKBH5#1   siALKBH5#3

F

Figure 7

A

CDKN1A

TIMP3

E2F1

CCNG2

B

24351 genes on microarray → Overlapped DEGs between two siRNAs

129 genes → Literature search for cell proliferation promoting function

10 genes → Expression qPCR

6 genes → MeRIP qPCR

CDKN1A, TIMP3, E2F1, CCNG2

C

	PC9	A549	kDa
ALKBH5			50
TIMP3			20
p21			20
E2F1			50
CCNG2			50
p53			50
GAPDH			37

siALKBH5 #1   siALKBH5 #3   siNC

Figure 8

Figure 9

Table 1. Clinical characteristics based on ALKBH5 and FTO expression in non-small cell lung cancer
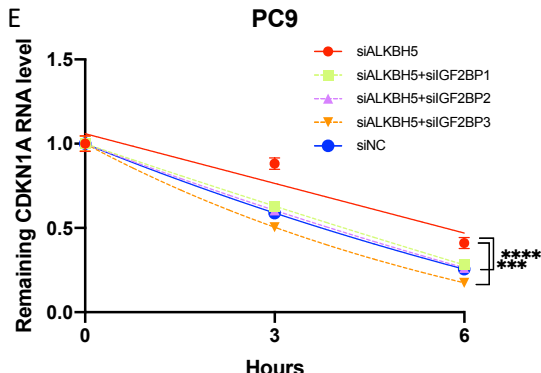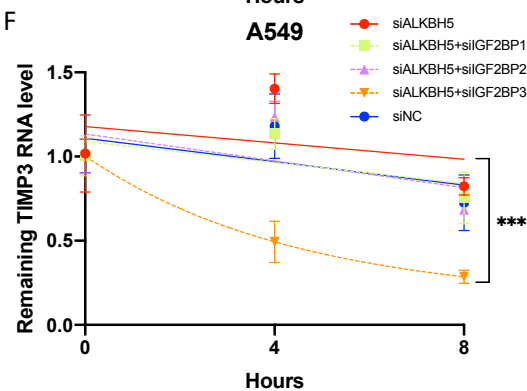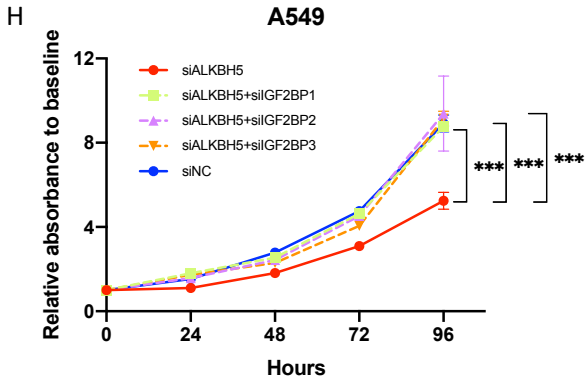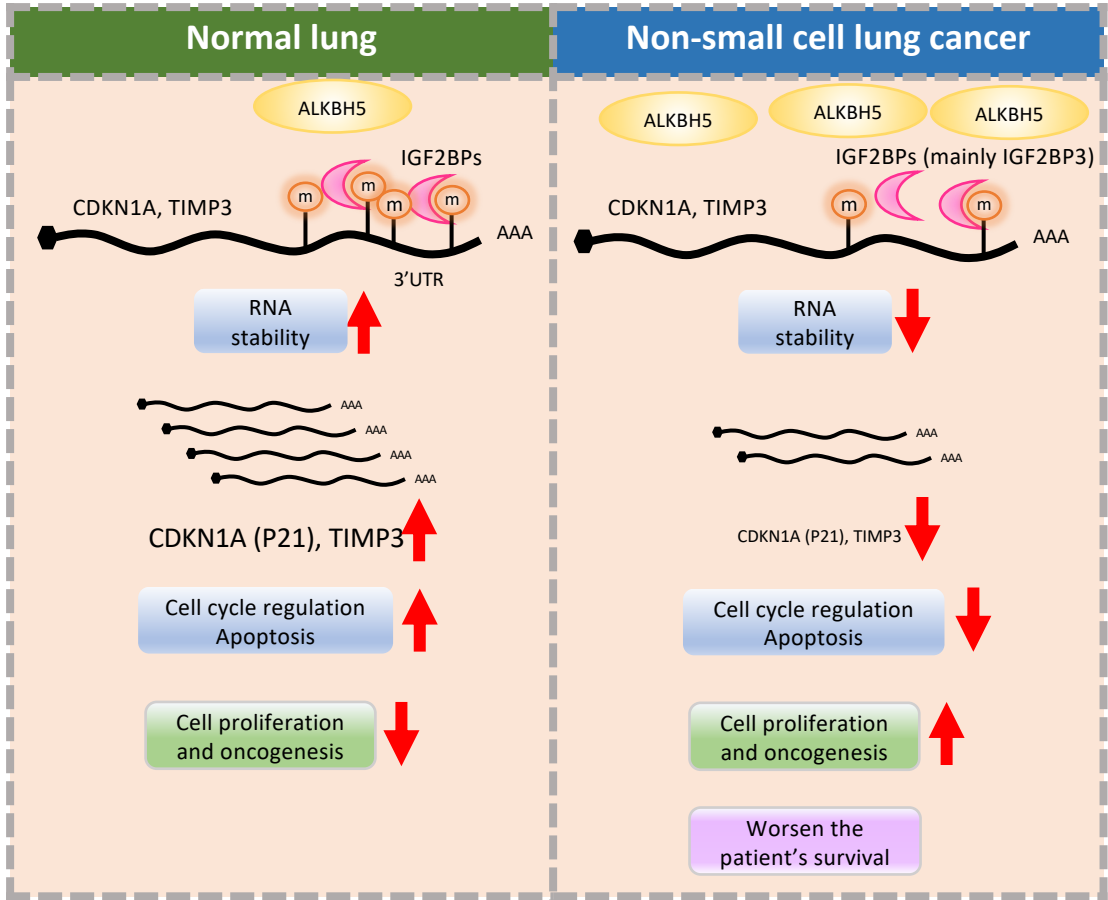
		ALKBH5			FTO		
	Total	low	high		low	high	
	N = 627	N = 315	N = 312	p-value	N = 313	N = 314	p-value
Age							
Median (range)	68 (23–88)	68 (23–88)	69 (39–85)	0.074	69 (23–88)	68 (34–85)	0.356
Sex, n (%)							
Male	430 (68.6)	214 (67.9)	216 (69.2)	0.732	223 (71.2)	207 (65.9)	0.169
Female	197 (31.4)	101 (32.1)	96 (30.8)		90 (28.8)	107 (34.1)	
Smoking history, n (%)							
Never	184 (29.3)	100 (31.7)	84 (26.9)	0.389	85 (27.2)	99 (31.5)	0.389
Ever	432 (68.9)	209 (66.3)	223 (71.5)		221 (70.6)	211 (67.2)	
Unkown	11 (1.8)	6 (1.9)	5 (1.6)		7 (2.2)	4 (1.3)	
Histology, n (%)							
Adenocarcinoma	413 (65.9)	205 (65.1)	208 (66.7)	0.151	204 (65.2)	209 (66.6)	0.184
Squamous cell carcinoma	170 (27.1)	93 (29.5)	77 (24.7)		92 (29.4)	78 (24.8)	
Others	44 (7.0)	17 (5.4)	27 (8.7)		17 (5.4)	27 (8.6)	
Tumor status, n (%)							
1	255 (40.7)	138 (43.8)	117 (37.5)	0.149	145 (46.3)	110 (35.0)	0.002
2	273 (43.5)	123 (39.0)	150 (48.1)		114 (36.4)	159 (50.6)	
3	62 (9.9)	33 (10.5)	29 (9.3)		31 (9.9)	31 (9.9)	
4	37 (5.9)	21 (6.7)	16 (5.1)		23 (7.3)	14 (4.5)	
Node metastasis, n (%)							

0	467 (74.5)	252 (80.0)	215 (68.9)	0.003	245 (78.3)	222 (70.7)	0.004
1	69 (11.0)	28 (8.9)	41 (13.1)		27 (8.6)	42 (13.4)	
2	84 (13.4)	30 (9.5)	54 (17.3)		38 (12.1)	46 (14.6)	
3	7 (1.1)	5 (1.6)	2 (0.6)		3 (1.0)	4 (1.3)	
Pathological stage, n (%)							
1	395 (63.0)	213 (67.6)	182 (58.3)	0.055	211 (67.4)	184 (58.6)	0.034
2	111 (17.7)	49 (15.6)	62 (19.9)		44 (14.1)	67 (21.3)	
3	121 (19.3)	53 (16.8)	68 (21.8)		58 (18.5)	63 (20.1)	
Chemotherapy, n (%)							
+	258 (41.1)	102 (32.4)	156 (50.0)	<0.001	77 (24.6)	181 (57.6)	<0.001
-	369 (58.9)	213 (67.6)	156 (50.0)		236 (75.4)	133 (42.4)	
EGFR mutation with IHC, n (%)							
Wild type	500 (79.7)	266 (84.4)	234 (75.0)	0.004	269 (85.9)	231 (73.6)	<0.001
Mutant	127 (20.3)	49 (15.6)	78 (25.0)		44 (14.1)	83 (26.4)	

Differences between experimental groups were assessed using Mann–Whitney U-test for continuous variables or Fisher's exact test for categorical data. Data represent median (range) or number (n) (%). IHC; immunohistochemistry

Table 2. Multivariate Cox hazards models of survivals in all patients with non-small cell lung cancer

Variable	Per unit for HR	Univariate analysis			Multivariate analysis		
		HR	95% CI	*p*-value	HR	95% CI	*p*-value
Age	1-year	1.023	1.007–1.040	0.005	1.039	1.019–1.060	<0.001
Sex	Male/Female	0.406	0.275–1.446	<0.001	1.267	0.686–2.331	0.447
Smoking status	Ever/Never	3.101	2.009–4.786	<0.001	3.024	1.510-6.053	<0.001
Histology	Ad to Sq	2.008	1.446–2.790	<0.001	1.116	0.766–1.625	0.568
Stage	1-stage	2.127	1.795–2.521	<0.001	2.307	1.943–2.739	<0.001
EGFR	mutant/wild	0.589	0.379–0.914	0.018			
chemotherapy	+/−	1.054	0.776–1.431	0.736			
ALKBH5	High to Low	1.675	1.230–2.521	0.001	1.468	1.039–2.073	0.029
FTO	High to Low	1.222	0.900–1.659	0.2			

Prediction of mortality of patients with non–small-lung cancer. The univariate and multivariate Cox proportional hazards models were applied to generate the hazard ratios (HRs) of death. Multivariate analysis was adjusted by age, sex, smoking status, histology, stage, and ALKBH5. HR; hazard ratio, CI; confdence interval, Ad; adenocarcinoma, Sq; squamous cell carcinoma